The LaRonde Penna World-Class Au-Rich Volcanogenic Massive Sulfide Deposit, Abitibi, Québec: Mineralogy and Geochemistry of Alteration and Implications for Genesis and Exploration*

B. DUBÉ,[†] P. MERCIER-LANGEVIN,

Geological Survey of Canada, 490 rue de la Couronne, Québec, Canada G1K 9A9

M. HANNINGTON,[**]

Geological Survey of Canada, 601 Booth Street, Ottawa, Ontario, Canada K1A 0E8

B. LAFRANCE,[***]

Ministère des Ressources naturelles, de la Faune, 82 boul. Québec, Rouyn-Noranda Québec, Canada J9X 6R1

G. GOSSELIN,

Agnico-Eagle Mines Ltd., Division Exploration, Val-d'Or, Québec, Canada J9P 4N9

AND P. GOSSELIN

Geological Survey of Canada, 490 rue de la Couronne, Québec, Canada G1K 9A9

Abstract

Gold-rich volcanogenic massive sulfide (VMS) deposits consist of synvolcanic banded and concordant massive sulfide lenses and adjacent stockwork feeder zones in which gold concentration in g/t Au exceeds the combined Cu, Pb, Zn grades in wt percent and thus constitutes the main commodity. The Agnico-Eagle LaRonde Penna deposit is a world-class Au-rich VMS (production, reserves and resources of 58.8 Mt at 4.31 g/t Au) located in the eastern part of the Blake River Group of the Abitibi greenstone belt. The deposit comprises four stacked massive sulfide lenses within the upper member of the Bousquet Formation (2698–2697 Ma). The two main ore zones, 20 North and 20 South, are sheetlike, massive to semimassive polymetallic sulfide lenses and stringer zones. Both lenses and sulfide stringers are deformed and transposed by the main foliation. The 20 North lens (Zn-Au-Ag-Cu-Pb) is the main orebody. It is subdivided into two zones: the 20N Au and 20N Zn zones. The 20N Au zone is a transposed and ribbon-textured gold- and copper-rich pyrite-chalcopyrite stringer zone overlain to the south by a 10- to 30-m-thick massive pyrite-sphalerite-galena lens (20N Zn zone). The 20 South lens is an 8- to 10-m-thick gold- and zinc-rich massive sulfide and stringer zone located about 10 to 15 m below the Cadillac Group sedimentary rocks (<2687 Ma). At depth (≥1,900 m below surface), the 20 North and 20 South lenses grade into aluminous zones composed mainly of quartz-pyrite-kyanite-andalusite-muscovite-Zn–rich staurolite assemblages that host transposed sulfide stringers and local semimassive to massive Au-rich pyrite and chalcopyrite layers.

The synvolcanic hydrothermal alteration now corresponds to mappable upper greenschist-lower amphibolite–grade metamorphic assemblages. The footwall of the 20 North lens is characterized by a large discordant to semiconformable distal quartz-biotite ± garnet assemblage, which transitions laterally into a proximal quartz-garnet-biotite-muscovite zone. The abundance of pink Mn-rich garnet porphyroblasts increases toward the 20N Au zone. The hanging wall of the 20 North lens is characterized by a meter-thick zone of fracture-controlled pink alteration composed of quartz, biotite, rutile and/or anatase, and titanite associated with barren sulfide stringers.

The garnet-rich assemblage in the footwall records gains in MnO, $Fe_2O_{3(total)}$, and MgO and losses of Na_2O. In the hanging wall, $Fe_2O_{3(total)}$, S, and CO_2 were added to the rocks with a slight increase in K_2O, and CaO. At depth (≥1,900 m), the Au-rich aluminous replacement zone is a (up to 30 m) thick, highly strained zone composed of a quartz-pyrite-kyanite-andalusite-chalcopyrite-gold assemblage. All oxides except Al_2O_3, SiO_2, and $Fe_2O_{3(total)}$ were strongly leached. The metamorphosed hydrothermal alteration associated with the 20 South lens is characterized by a pink quartz-biotite-rutile-titanite assemblage very similar to that in the hanging wall of the 20 North lens. Toward the ore zone, the pink assemblage is gradually replaced by a proximal quartz-muscovite-green mica-pyrite assemblage, which hosts the sulfide mineralization.

The aluminous alteration at LaRonde Penna is interpreted to be the metamorphic equivalent of an advanced argillic alteration and has many similarities to that of metamorphosed high-sulfidation systems and particularly

---

*Geological Survey of Canada contribution no. 20060353.

[†] Corresponding author: e-mail, bdube@nrcan.gc.ca

**Present address: University of Ottawa, 140 Louis Pasteur, Ottawa, Canada ON K1N 6N5.

***Present address: Cogitore Resources Inc., 1300 Saguenay, Suite 200, Rouyn-Noranda, Québec, Canada J9X 7C3.

a class of Au-rich VMS characterized by aluminous alteration. The LaRonde Penna and Bousquet 2-Dumagami deposits are interpreted to represent one large hydrothermal system in which variable contributions of hydrothermally modified seawater and magmatic volatiles contributed to the different styles of alteration and mineralization.

The study illustrates that diverse styles of Au-rich VMS can coexist within the same deposit. In terms of exploration, almost all sulfide lenses or hydrothermal alterations minerals are located at or near volcanic hiatuses within the Bousquet Formation. These hiatuses represent major exploration targets especially when located in the upper part of the Bousquet Formation. The aluminous alteration zones have accommodated most of the postore strain due to their ductility and are transformed into schists. Consequently, the alteration product coincides spatially with the deformation zones despite the lack of a genetic relationship. Quartz-and Mn-rich garnet-biotite assemblages and/or aluminous schists with anomalous gold and/or zinc in intermediate to felsic transitional to calc-alkaline volcanic or volcaniclastic rocks located underneath a sedimentary cover represent excellent targets for Au-rich VMS in metamorphosed terranes.

Introduction

GOLD-RICH volcanogenic massive sulfide (VMS) deposits are important gold deposits in a strict economic sense (Poulsen et al., 2000). Like other VMS deposits they consist of synvolcanic banded and locally concordant massive sulfide lenses and adjacent discordant stockwork feeder zones. In these deposits, gold concentration (in g/t) exceeds the combined Cu, Pb, Zn grades in wt percent and thus constitutes the main commodity (Poulsen and Hannington, 1995; Poulsen et al., 2000). Many gold-rich VMS deposits occur in deformed and metamorphosed greenstone belts of various ages and may contain local syntectonic quartz-sulfide or rarely quartz-tourmaline veins, which can complicate the interpretation of their paragenesis. The timing of gold deposition (synvolcanic or syntectonic) relative to the formation of the massive sulfide orebody is therefore the subject of much debate, particularly in metamorphosed Precambrian terranes (Valliant and Hutchinson, 1982; Stone et al., 1988; Arnold and Sillitoe, 1989; Poulsen and Hannington, 1995; Bergman-Weihed et al., 1996; Sillitoe et al., 1996; Hannington et al. 1999; Huston, 2000). It has been proposed that syngenetic volcanic-hosted, gold-poor base metal mineralization in some Archean examples was overprinted by syndeformation Au mineralization (Tourigny et al., 1989; Marquis et al, 1990a-c; Yeats and Groves, 1998).

Although there are only a few world-class examples, the Au-rich polymetallic nature of these deposits makes them an attractive exploration target. The world production and reserves for Au-rich VMS deposits are 1,370 metric tonnes (t) Au, equivalent to 1.2 percent of the world lode gold production and reserves, including the Witwatersrand (120,689 t Au: Gosselin and Dubé, 2005a). Production and reserves of Canadian Au-rich VMS gold deposits are 870 t, which constitutes close to 10 percent of the total production and reserves from Canadian lode gold deposits (9,280 t Au: Gosselin and Dubé, 2005b).

Agnico-Eagle's LaRonde Penna deposit (Fig. 1) is the largest gold mine currently in operation in Canada. Production from the LaRonde Penna shaft began in April, 2000. More than 12 Mt of ore at 3.53 g/t Au (1.4 Moz of gold), 2.66 percent Zn, 0.28 percent Cu, and 53.7 g/t Ag have already been extracted from the beginning of its production to 2005. Reserves and global resources as of December 31, 2005 were 6.7 Moz Au from more than 46 Mt at an average grade of 4.51 g/t Au, 2.04 percent Zn, 0.33 percent Cu, and 42.7 g/t Ag. LaRonde Penna is the second largest Au-rich VMS deposit, after the Horne deposit in Noranda, which produced 331 t Au (Gosselin and Dubé, 2005b). Although Au-rich VMS deposits represent a key exploration target, detailed deposit-scale studies of this style of mineralization are limited. The LaRonde Penna deposit represents a key deposit in this context and an opportunity to contribute to the understanding of this deposit type.

The LaRonde Penna deposit is located 1 km east of the Bousquet 2-Dumagami deposit in the eastern part of the Doyon-Bousquet-LaRonde mining camp, which contains more than 22.3 Moz Au (past production, reserves, and resources; Fig. 1). The Au-rich VMS deposits in the district are hosted by the upper portion of the Bousquet Formation of the Blake River Group (Lafrance et al., 2003; Mercier-Langevin et al., 2004; Mercier-Langevin, 2005). The Blake River Group also hosts the VMS deposits located in the nearby world-class Noranda district, including two notably Au-rich VMS deposits, Horne (331 t Au) and Quemont (66 t Au; Gosselin and Dubé, 2005b), and 17 other polymetallic Cu-Zn ± Au VMS deposits.

A synthesis of the Doyon-Bousquet-LaRonde mining district was undertaken in the summer of 2000 as a joint effort involving the Ministère des Ressources naturelles, de la Faune du Québec, the Geological Survey of Canada, Cambior Inc., Barrick Gold Corp., Agnico-Eagle Mines Ltd., Ressources Yorbeau Ltd., Institut national de la recherche scientifique (INRS-ETE), and the Université du Québec à Chicoutimi. The primary objective was to better understand the regional and deposit-scale geologic characteristics of the district. Part of the results were published in a series of Quebec government reports (Lafrance et al., 2003, Dubé et al., 2004; Mercier-Langevin et al., 2004).

This paper accompanies two contributions by Mercier-Langevin et al. (2007a, b), which respectively describe the geology and geochronology and lithogeochemistry and paleotectonic setting of the LaRonde Penna deposit. Here, we summarize the mineralogical and lithogeochemical signatures of the hydrothermal system(s) of the LaRonde Penna deposit, discuss the timing of gold introduction, and investigate a genetic model for Au-rich VMS deposits, as well as exploration implications in the district and elsewhere in greenstone belts. The study also demonstrates that distinctive Zn-Au and Cu-Au metal associations and diverse alteration types can coexist laterally within a single VMS deposit.

Regional Geologic Setting

The Doyon-Bousquet-LaRonde gold district is located 45 km east of Rouyn-Noranda in the late Archean southern
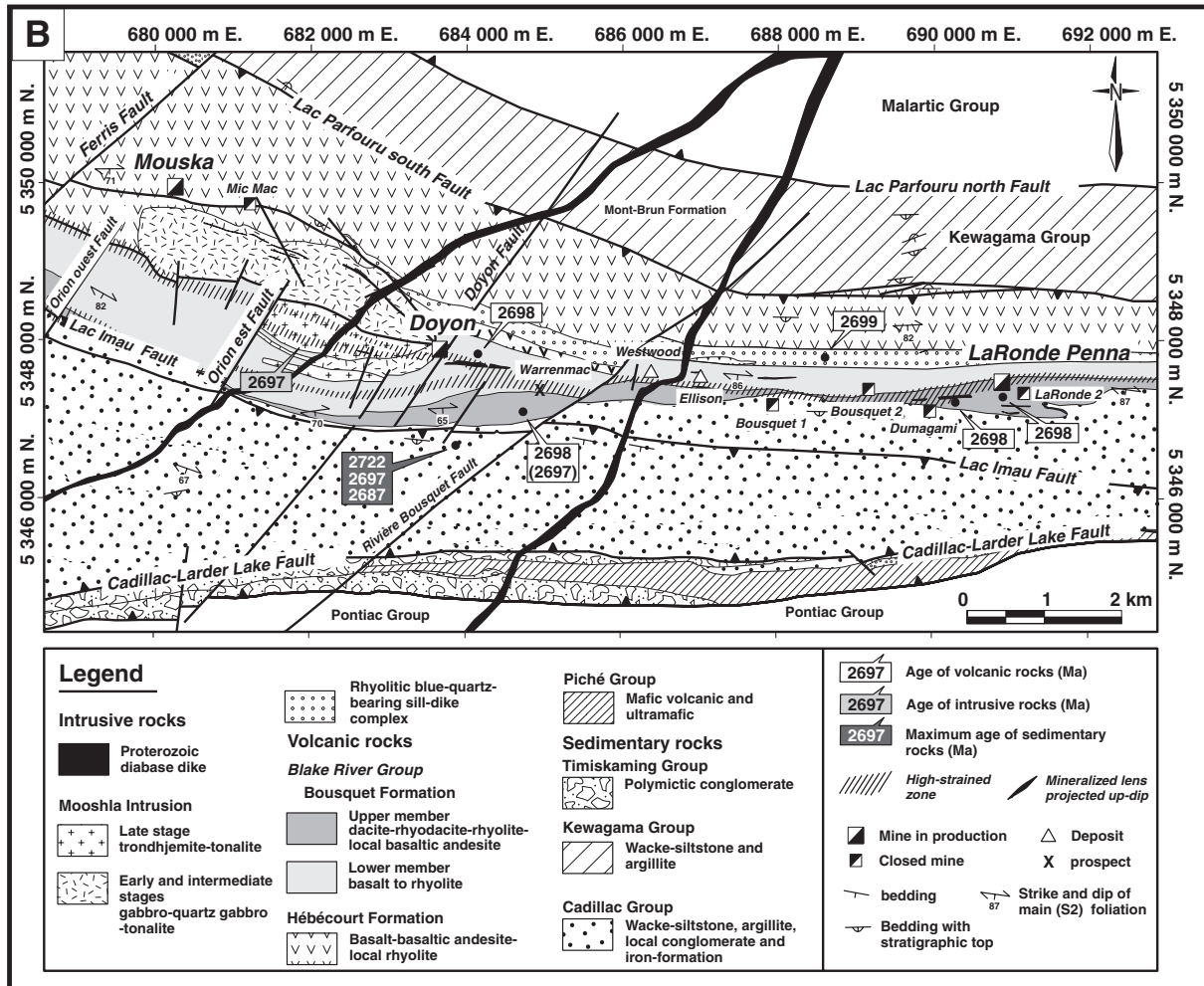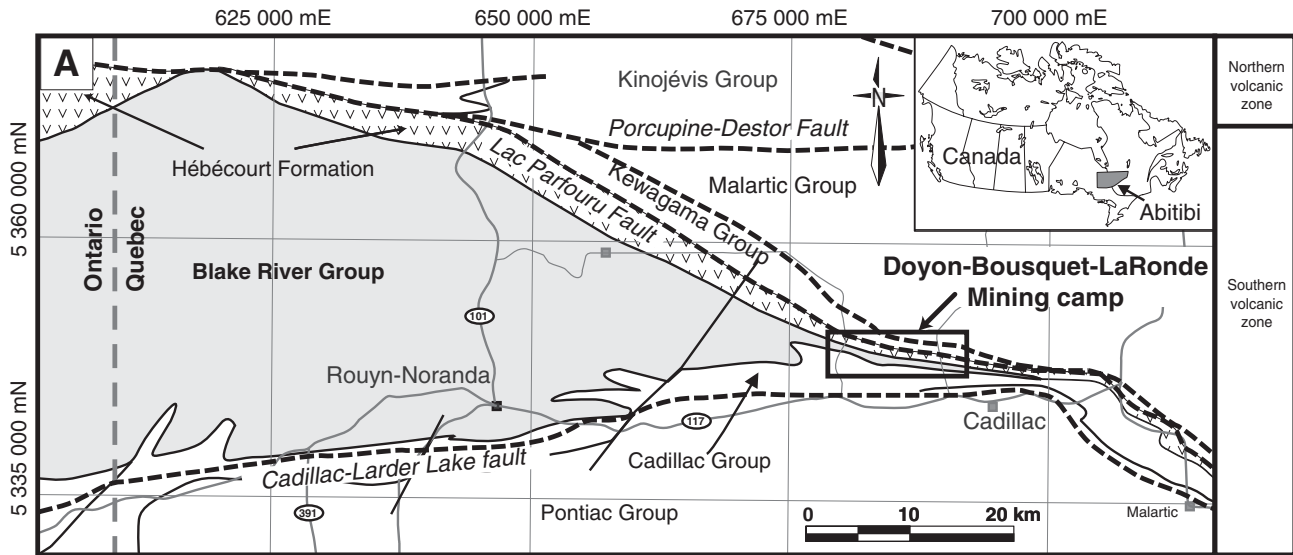
FIG. 1. A. Location of the Doyon-Bousquet-LaRonde mining camp, Blake River Group, which includes the Bousquet Formation. The inset shows the location of the Abitibi greenstone belt. B. Simplified geology of the Doyon-Bousquet-LaRonde mining camp (modified from Lafrance et al., 2005). U-Pb age from Lafrance et al. (2005) and Mercier-Langevin et al., 2007a)

Abitibi greenstone belt of the Superior province of the Canadian Shield (Fig. 1A). The northern portion of the volcanic succession consists of the Hébécourt Formation which extends to the west to the Québec-Ontario border (Fig. 1A). The Hébécourt Formation consists of laterally extensive tholeiitic basalt and basaltic andesite flows, cogenetic gabbroic sills, and small isolated rhyolite flows. The Bousquet Formation, which hosts most of the deposits, stratigraphically overlies the Hébécourt Formation. The Bousquet Formation is part of the Blake River Group and constitutes a south-facing homoclinal sequence which is subdivided into lower (2699–2698 Ma) and upper members (2698–2697 Ma; Lafrance et al., 2003, 2005; Mercier-Langevin et al., 2004). Both of these members consist of basaltic to rhyolitic flows, domes, synvolcanic intrusions, and volcaniclastic strata. The lower member is characterized by regionally extensive units whereas the upper member is composed of localized domes and associated volcaniclastic facies. These isolated volcanic units mark the location of three different volcanic centers, including the Doyon and LaRonde centers (Lafrance et al., 2003). In terms of lithogeochemistry, the Bousquet Formation is a continuous differentiated volcanic suite from basalt to rhyolite, including an important volume of dacite and rhyodacite (Lafrance et al., 2003). The latter is a distinctive feature of the Bousquet Formation in comparison to the bimodal basalt and/or rhyolite suites observed elsewhere in the Blake River Group (e.g., Noranda camp: Gibson and Watkinson, 1990). The lower member of the Bousquet Formation is tholeiitic to transitional, whereas the upper member is transitional to calc-alkaline (Lafrance et al., 2003; Mercier-Langevin et al., 2004, 2007b). To the south, the sedimentary rock-dominated Cadillac Group overlies the Bousquet Formation along a nondepositional disconformity (<2687 Ma; Davis, 2002), which marks a depositional hiatus of at least 7 Ma (Mercier-Langevin et al., 2007a).

A tholeiitic to transitional, rhyolitic, blue quartz-bearing sill-dike complex (2699 ± 1.5 Ma) intruded the interface between the Hébécourt Formation and an intermediate scoriaceous tuff at the base of the lower member of the Bousquet Formation (Lafrance et al., 2003). The thickest portion of this sill-dike complex is centered underneath the Bousquet 1 and 2 and the Dumagami mines (Fig. 1B). To the west, the Mooshla pluton was emplaced along the same interface and into the lower member of the Bousquet Formation. The Mooshla intrusion is composed of three differentiated intrusive stages: (1) early tholeiitic to transitional dioritic sills, (2) an intermediate tholeiitic to transitional gabbro-tonalite suite that forms the northern half of the intrusion (stages 1 and 2 combined in Fig. 1B), and (3) a late (2697 Ma) transitional to calc-alkaline trondhjemitic suite, representing the upper part of the intrusion (Galley et al., 2003; Lafrance et al., 2003 and references therein). The middle stage mafic-intermediate suite is coeval with the lower member of the Bousquet Formation, and the later trondhjemitic suite is contemporaneous and possibly comagmatic with the upper member of the Bousquet Formation and could represent the intrusive equivalent to the rhyodacite unit (Valliant and Hutchinson, 1982; Dubé et al., 2003, Mercier-Langevin, 2005). The structurally controlled Mouska deposit is partially hosted within the early Mooshla intrusive suite, and
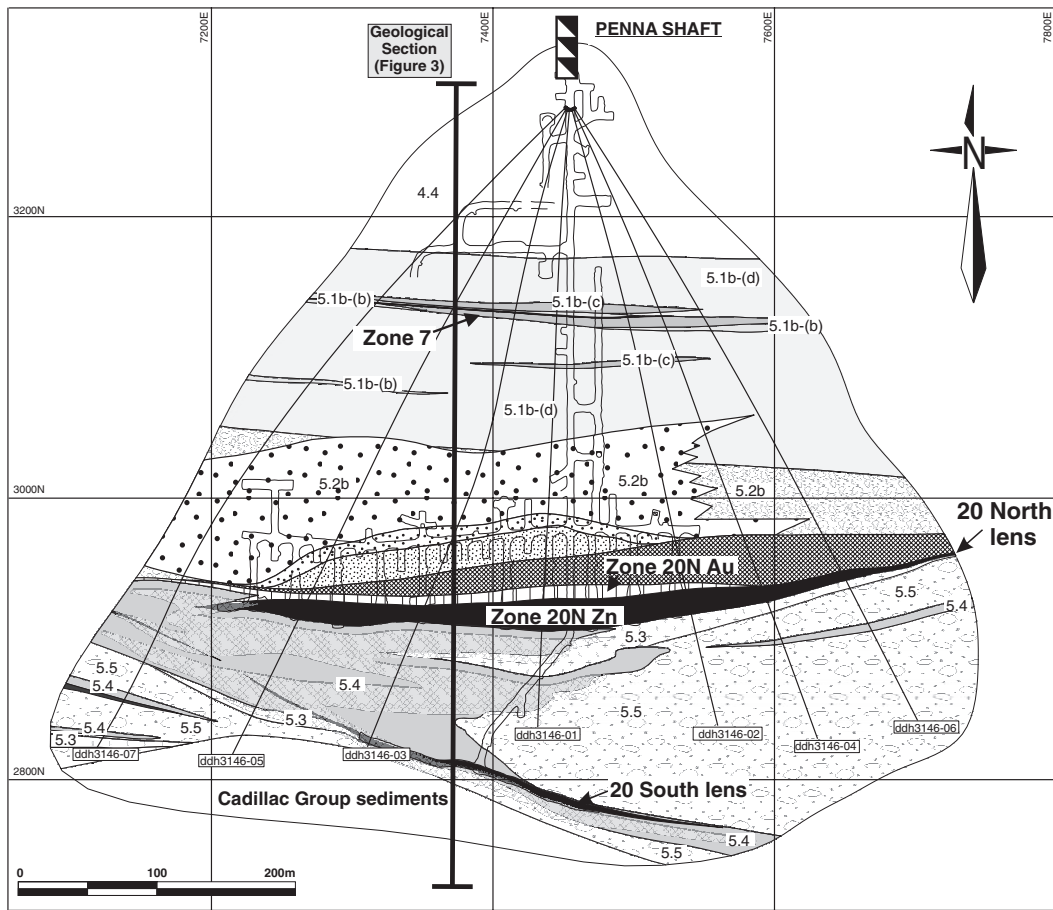
parts of the Doyon intrusion-related Au deposit occur within the later trondhjemitic suite (Gosselin, 1998; Galley et al., 2003).

The Blake River Group is characterized by three main stages of deformation mainly related to north-south convergence, followed by oblique dextral shearing (Dimroth et al., 1983; Hubert et al., 1984, Tourigny et al., 1988; Marquis et al., 1990a, Mercier-Langevin et al., 2007a). The regional D_1 structures are not observed in the LaRonde Penna mine area. The main deformation recorded by the rocks at the LaRonde Penna deposit is attributed to D_2 within the Blake River Group (Dimroth et al., 1983, Hubert et al., 1984) and is represented by a steeply dipping east-west–trending foliation (S_2) with associated subvertical folds (F_2) and a moderately to steeply west-plunging stretching lineation (L_2). In the deposit area, D_2 was followed by D_3 which is characterized by a northeast-southwest–trending cleavage (S_3), small-scale folds (F_3), and a conjugate set of northeast-southwest (sinistral) and northwest-southeast (dextral) faults (Mercier-Langevin et al., 2007a). The late deformation D_4 is characterized by conjugate sets of northwest- and northeast-trending fractures, crenulation cleavages, and kink bands; these features are documented in the Bousquet 1 and Bousquet 2-Dumagami deposits (Tourigny et al., 1989; Marquis et al., 1990a; Teasdale et al., 1996, Mercier-Langevin et al., 2007a). Regional metamorphism in the Doyon-Bousquet-LaRonde district area reached the upper greenschist-lower amphibolite transition and then underwent retrogressive regional metamorphism to lower greenschist grade (Stone, 1988; Stone et al., 1988; Tourigny et al., 1989; Marquis et al., 1990a; Powell et al., 1995; Mercier-Langevin et al., 2004).

Deposit Geology

The LaRonde Penna deposit is located <1 km east of the Bousquet 2-Dumagami orebody (Fig. 1B) and together they form a cluster of deposits informally named the LaRonde-Bousquet 2 Au-rich VMS complex (Dubé et al., 2003, 2004). A brief summary of the geologic setting of the LaRonde Penna deposit is presented below. Readers are referred to Mercier-Langevin et al. (2007a) for more details. The LaRonde Penna Au-rich VMS deposit consists of four stacked massive sulfide lenses within the upper member of the Bousquet Formation. A strong north-south–directed shortening (D_2) is responsible for transposition, strong flattening, and minor folding of the units and sulfide lenses at the deposit scale.

The various massive sulfide lenses sit on, or are hosted by, volcanic rocks of the upper member of the Bousquet Formation, which is subdivided into five units from north to south (Fig. 2: Lafrance et al., 2003; Mercier-Langevin et al., 2004). Unit 5.1, host to the two lowermost lenses, zones 6 and 7 (Fig. 3), consists of transitional to calc-alkaline dacitic to rhyodacitic domes and flow breccias (unit 5.1b-d) and thin andesitic horizons (unit 5.1b-b). The overlying unit (5.2b) is composed of rhyodacitic to rhyolitic calc-alkaline domes and/or flow breccia mainly developed in the LaRonde Penna area. Unit 5.2b hosts, at least in part, the 20 North lens. This unit is capped and intruded by thin layers of calc-alkaline, feldspar- and quartz-phyric rhyolite flows and sills (unit 5.3), and/or by "basaltic andesite" (high-level sills and dikes of

FIG. 2. Geology of the LaRonde Penna deposit level 146 (1,460 m below surface), showing the distribution of the mineralized and altered rocks (modified from Dubé et al., 2004). Numbers such as 4.4 and 5.5 are unit numbers (see text).

microgabbro to diorite; unit 5.4). Units 5.3 and 5.4 are interdigitated with, or have been emplaced into, rhyodacitic to rhyolitic volcanic flow-breccia deposits of unit 5.5. The 20 South lens is mainly hosted in rocks of units 5.4 and 5.5 (Fig. 2). Toward the west, the Bousquet 2-Dumagami orebody is hosted by the feldspar- and quartz-phyric rhyolite (unit 5.3), near the interface with dacitic volcaniclastic rocks (Unit 5.1) located in the stratigraphic footwall. The volcanic sequence of

the Bousquet Formation is overlain by wacke units of the Cadillac Group (Figs. 1, 3).

Mineralized Zones

The two main ore zones at LaRonde Penna are the 20 North and 20 South lenses. These are sheetlike, massive to semimassive polymetallic sulfide lenses. The 20 North lens is characterized by a Zn-Au-Ag-Cu-Pb assemblage and represents
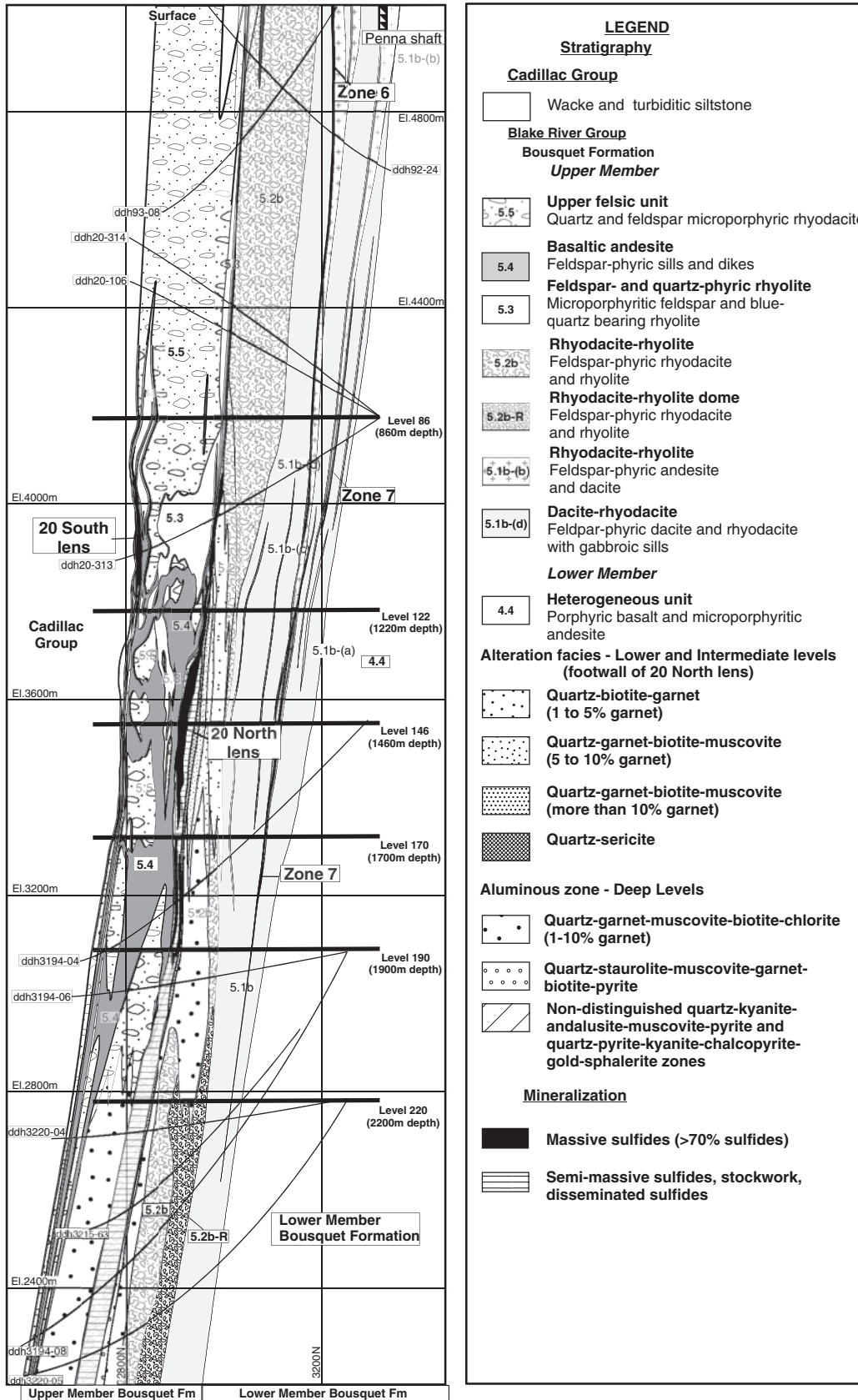
FIG. 3. Section 7380E of the LaRonde Penna deposit, showing the stratigraphy and the distribution of the mineralized and altered rocks (modified from Mercier-Langevin, 2005).

about 85 percent of the known gold reserves and resources. It is stratigraphically below the 20 South Au-Zn-Ag-Cu-Pb lens and above the two smaller Au-Ag-Cu-Zn lenses (zones 6 and 7; Fig. 3). Although deformed and metamorphosed, metal zonation within the lenses is characterized by the typical upward enrichment of Zn and Pb in VMS deposits, indicating stratigraphic tops toward the south-southeast. This interpretation is consistent with previous stratigraphic and structural work in the district (Gunning, 1941; Valliant and Barnett, 1982; Stone, 1990). The ore lenses and sulfide stringers have been strongly deformed and transposed by the main foliation (S_2). The sulfide minerals show recrystallization textures typical of upper greenschist-lower amphibolite facies metamorphism, including total annealing and remobilization (Dubé et al., 2004). Deformation-induced mineralogical banding and folding of the sulfide and argillite layers are common. Chalcopyrite is commonly remobilized and associated with visible gold that coats or fills late fractures. The presence of chalcopyrite in the ore zone is generally an indication of higher gold grade.

20 North lens

The 20 North lens has a known vertical extent of 2,300 m (levels 70–300) and lateral extent of 600 m (Figs. 2, 3). In the upper and intermediate parts of the mine, the lens is up to 40 m thick and is subdivided into two zones: the 20N Au and 20N Zn zones. The 20N Au zone is characterized by a 5- to 10-m-thick, strongly transposed and ribbon-textured gold- and copper-rich pyrite-chalcopyrite stringer zone in a quartz-plagioclase-muscovite-pyrite ± chlorite matrix with local massive sulfide zones (Fig. 4A, B). It is overlain to the south by a 10- to 30-m-thick massive pyrite-sphalerite-galena lens (20N Zn zone) composed of massive pyrite with millimeter- to centimeter-thick sphalerite-rich bands and minor quartz, muscovite, and local galena toward the upper part (Fig. 4C).

The 20 North lens occurs at the contact between the hanging-wall basaltic andesite (5.4) or rhyolite (5.3) and the rhyodacite-rhyolite flow breccia (5.2) in the footwall (Fig. 2). The lens was formed, at least in part, by replacement of the upper portion of unit 5.2 as suggested by the presence of clasts of the 5.2 rhyodacite within the ore zone (Mercier-Langevin et al., 2007a). Locally, the 20N Au and 20N Zn zones are separated by a meter-thick barren to low-grade interval of coarse pyrite and quartz that has replaced the rhyodacite breccia. Dismembered and transposed black argillites with scattered pyrite nodules are present toward the upper part of the 20N Zn zone (Fig. 4D).

20 South lens

The 20 South lens is an 8- to 10-m-thick gold- (up to 30 g/t Au) and zinc-rich sulfide lens composed of pyrite, chalcopyrite, sphalerite, and pyrrhotite emplaced toward the top of unit 5.4 (mafic sills). This lens is generally located about 10 to 15 m below (to the north of) the Cadillac Group sedimentary strata (Fig. 2). However, the massive sulfide lens is locally in contact with the sedimentary strata. The lens is up to 200 m wide and has a known vertical extent of at least 1,300 m (Fig. 3), from a 900- to 2,180-m depth. The economic mineralization is mainly concentrated in two zones: at a 900- to 1,580-m depth and at a 1,700- to 2,180-m depth (Figs. 2,

3). The massive sulfide portion of the 20 South lens in the upper part of the mine (level 106, 1,060-m depth) hosts the highest Au grades (10–30 g/t Au) of the entire deposit. Elsewhere, the mineralized zone consists of centimeter- to meter-wide Au- and Zn-rich massive sulfides with pyrite-pyrrhotite-sphalerite-chalcopyrite ± galena stringers transposed by the main foliation within a strongly foliated quartz-plagioclase-muscovite-green mica-chlorite-titanite and/or anatase schist (Fig. 4E). Sphalerite and galena are concentrated toward the upper part (south portion) of the lens. The 20 South lens is slightly discordant to the ore-hosting lithologic units and suggests that it was formed, at least in part, by replacement. Toward the center of the deposit, the lens is hosted by the basaltic andesite, whereas to the east the ore is hosted by the rhyodacitic to rhyolitic flow-breccia unit (5.5), which is present in both the footwall and hanging wall (Fig. 2).

Zones 7 and 6

Zones 7 and 6 are two small massive sulfide lenses mined from the LaRonde 2 shaft at less than 450 m from the surface. Only the distal expression of these massive sulfide lenses is accessible at LaRonde Penna. Zone 7 is hosted by rocks within a high-strain zone about 10 to 25 m above the contact between basaltic and andesitic flows (unit 4.4) and dacite-rhyodacite with associated basaltic andesite sills and dikes (unit 5.1b; Fig. 2). Zone 7 forms an extensively altered interval that can be traced along strike for at least a few kilometers. It is characterized by meter-wide quartz-muscovite schists with transposed stringers and local semimassive pyrite with minor sphalerite and chalcopyrite. Zone 6 is up to 25 m wide and is hosted within the 5.1b dacite-rhyodacite unit. It is located 10 to 30 m stratigraphically above (to the south) of zone 7 (Fig. 3). Like zone 7, it is a quartz-muscovite-pyrite schist containing stringers of pyrite-sphalerite with minor chalcopyrite transposed parallel to the main foliation (S_2). Locally, zones 7 and 6 contain a few meters thickness of massive sulfide composed of pyrite with minor sphalerite and traces of chalcopyrite (Fig. 4F).

Mineralized zones at depth

At depth ($\geq$ 1,900 m below surface), the 20 North and 20 South lenses and zones 6 and 7 grade into sulfide-rich aluminous zones. This is particularly well illustrated by the 20 North ore zone, which transitions downdip into a Au-rich zone composed mainly of quartz-pyrite-kyanite-andalusite-muscovite schist that hosts transposed sulfide stringers and local semimassive to massive Au-rich pyrite and chalcopyrite layers (Fig. 4G). Sphalerite occurs locally toward the top of the lens. One 31-m-wide mineralized zone in DDH 3206-14D grades 6.03 g/t Au, 15.1 g/t Ag, 0.49 percent Cu, and 0.03 percent Zn (Dubé et al., 2004).

Pyrrhotite at the contact between the Blake River and the Cadillac Groups

A semimassive deformed and brecciated pyrrhotite-rich horizon commonly marks the contact between the uppermost unit 5.5 of the Bousquet Formation and the overlying Cadillac Group graywacke, stratigraphically above the 20 South lens (Dubé et al., 2004) (Fig. 4H). Taking into account the age of the Bousquet Formation upper member (2698–2697
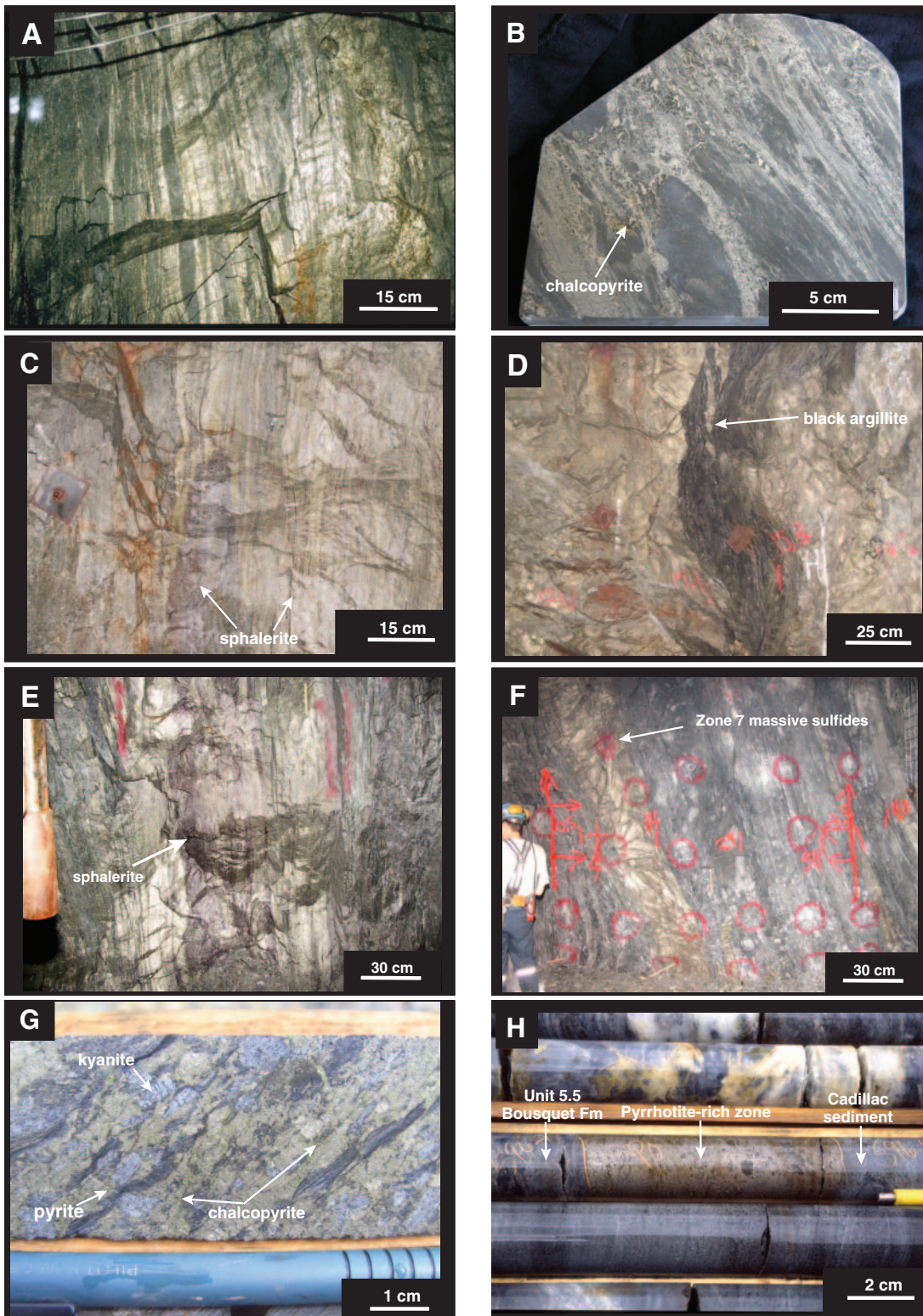
FIG. 4. A. Section view of the 20N Au zone, showing strong transposition of the pyrite- and chalcopyrite-rich veins parallel to the main foliation (stope 118-20-72). B. Sample from the 20N Au zone, showing the intensity of the postore deformation. C. Transposed sphalerite layers within massive pyrite, 20N Zn zone (section view, stope 152-20-66). D. Highly strained black argillite enclave within the 20N Zn zone (section view, stope 152-20-66). E. Close up of the 20 South lens, showing transposed sphalerite layer in massive pyrite (section view, stope 106-21-80). F. Section view of zone 7, showing massive sulfides transposed parallel to the main foliation. G. Foliated aluminous 20N Au zone at depth in the mine showing kyanite, pyrite, and chalcopyrite. H. Pyrrhotite-rich semimassive sulfide zone at the contact between unit 5.5 of the upper member of the Bousquet Formation and the Cadillac Group sedimentary rocks.

Ma) and the maximum age of the Cadillac Group (<2687 Ma), this contact probably corresponds to a strained unconformity. The sulfide-rich horizon is up to 30 cm thick and is composed of quartz, plagioclase, and biotite in a matrix of pyrrhotite and pyrite. It contains up to 0.14 percent Zn and 0.01 percent Cu but only traces of Au (Dubé et al., 2004). This pyrrhotite-rich horizon was reported at the Dumagami mine by Marquis et al. (1990a) and was interpreted as a mixed volcaniclastic and exhalite layer belonging to the Blake River Group. These authors also described the local presence of graphitic schists between the pyrrhotite-rich horizon and the Cadillac Group sediments. Disseminated pyrrhotite is also found in the graywacke up to 15 cm from the upper contact of the Bousquet Formation, along with biotite and local garnet and chloritoid.

Hydrothermal alteration zones

The mappable alteration zones at LaRonde Penna are metamorphic assemblages derived from synvolcanic hydrothermal alteration. Alteration minerals vary among the massive sulfide lenses and with depth. Petrography, lithogeochemistry, and whole-rock X-ray diffraction (XRD) have been used to characterize the hydrothermal alteration in terms of mineralogical assemblages and geochemistry.

Upper and intermediate levels of the 20 North massive sulfide lens

Mineralogy: The footwall of the 20 North lens in the upper and intermediate levels of the mine is characterized by a large discordant to semiconformable alteration zone within rhyodacitic to rhyolitic domes and flow breccia (unit 5.2b). The distal alteration zone (up to 100–130 m stratigraphically beneath the lens) is a quartz-biotite ± garnet assemblage which grades into a proximal quartz-garnet-biotite-muscovite alteration zone (within 30–50 m of the lens). The proximal alteration is 400 to 500 m wide and has a minimum vertical extent in the mine of 900 m (Figs. 2, 3). The distribution of the proximal quartz-garnet-biotite-muscovite alteration in the footwall of 20 North lens coincides with the location of the 20N Au zone in the upper and intermediate parts of the mine (Fig. 3). In addition to quartz, garnet, biotite, and muscovite, variable amounts of other minerals (Table 1) occur in a quartz-feldspar groundmass dominated by fine-grained recrystallized quartz. The abundance and size of garnet porphyroblasts increase toward the 20N Au zone. The garnet is pink (Fig. 5A) and varies in size from 1 mm to 1.5 cm, and it may represent up to 30 vol percent of the assemblage within 50 m of the 20N Au zone. The garnets forms syn- to late-deformation subhedral poikiloblasts elongated parallel to the main foliation (S2); Fig. 5B, C) and contain trails of gangue inclusions oriented parallel to the foliation (Fig. 5D). Microprobe analyses indicate that the garnet is Mn-rich Fe-Ca spessartine or almandine ($Mn_{1.4}$, $Fe_{3.2}$, $Ca_{1.14}$, $Mg_{0.16})_6$ Al_4 Si_6 O_{24} with up to 16.3 percent MnO (Table 2). Where abundant, the garnets occur in millimeter-wide bands of garnet-epidote-clinozoïsite-muscovite-pyrite ± pyrrhotite that may represent fracture-controlled alteration that is transposed by the foliation. Biotite is also relatively abundant (up to 25 vol %) and is commonly elongated parallel to the foliation. The abundance of biotite decreases toward the footwall of the massive sulfides where biotite is replaced (retrograded) by Mg-rich chlorite, muscovite, and locally chloritoid (Fig. 5B). Where present, the chloritoid forms unoriented late- to post-deformation porphyroblasts containing foliation-parallel quartz inclusions. Traces of tourmaline, anhydrite, and carbonate as well as transposed veinlets of quartz-clinozoïsite-chlorite-muscovite-pyrrhotite-pyrite-sphalerite are locally present.

Immediately beneath the massive sulfides the quartz-garnet-biotite-muscovite assemblage grades into a zone a few meters wide of quartz and muscovite (Fig. 5E). The presence and thickness of this zone increases to the east. In addition to quartz and muscovite, this assemblage contains plagioclase and many other minor to trace minerals and sulfides, including Mg chlorite, small garnets (≤1–5%), chloritoid, clinozoïsite, and margarite (Table 1). Transposed stringers containing these minerals, together with pyrite, pyrrhotite, sphalerite, and chalcopyrite also are common. Locally, a few meters of quartz-chloritoid-chlorite-muscovite occur between the quartz-garnet-biotite-muscovite and the quartz-muscovite zones.

The stratigraphic hanging wall of the 20 North lens is characterized by distinctive, meter-thick zones of fracture-controlled pink alteration associated with up to 20 percent sulfide stringers and confined to the massive basaltic andesite (5.4 unit; Fig. 5F, G). The abundance of stringers decreases away (to the south) from the 20N Zn zone massive sulfides. However, toward the west, this pink alteration forms a continuous zone that extends from the hanging wall of the 20N Zn zone to the footwall of the 20 South lens (Fig. 2). The sulfide stringers are transposed subparallel to the main foliation and are composed of pyrrhotite, pyrite, with traces of sphalerite ± chalcopyrite and variable amounts of quartz, albite, calcite, clinozoïsite, margarite, chlorite, Mg biotite, tourmaline, muscovite, and titanite. The pink coloration characteristic of this assemblage is caused by veinlets and disseminations of titanite and rutile + anatase with biotite and tourmaline as well as fine rutile + anatase dusting within the microphenocrysts of albite or within the matrix-forming plagioclase (Figs. 5G, H, 6A, B). Biotite is commonly distributed symmetrically on both sides of the rutile + anatase + tourmaline veinlets as well as disseminated in the matrix. Calcite (≤10%), and traces to a few percent other minerals, including sulfides, are also present (Table 1). Locally, the pink assemblage is replaced by a greenish-beige–colored assemblage characterized by millimeter- to centimeter-scale veinlets or bands of muscovite and tourmaline with quartz, pyrrhotite, pyrite, chalcopyrite, green micas, margarite, titanite, chlorite, and clinoizoisite. The veinlets are transposed into the main foliation, and muscovite forms selvages on both sides of the veinlets and disseminations in the quartz-feldspar matrix. Biotite is replaced by Mg chlorite. Here, the rutile-bearing albite has been recrytallized, and TiO_2 has been converted to titanite in the matrix, resulting in the loss of the pink coloration associated with the earlier alteration.

Lithogeochemistry: Table 3 lists representative geochemical analyses, from multiple locations in the deposit, of different alteration assemblages associated with the 20 North lens, as well as the average composition of the least altered rhyodacite to rhyolite host (unit 5.2b). A sharp change in Zr, TiO_2, and SiO_2 marks the boundary between the 5.2b unit and

TABLE 1. Summary of the Mineralogy and Mass Gains and Losses of the Various Metamorphosed Hydrothermal Alteration Assemblages at LaRonde Penna[1]

Main mineralogical assemblage	Associated minerals	Main chemical changes
A. 20 North lens: Upper and Intermediate levels		
(1) Footwall		
Quartz-garnet-biotite-Muscovite	chlorite, amphibole, pyroxene clinozoisite, epidote, ±chloritoid and anatase	Losses: Na_2O, K_2O, CO_2, V, Ba gains: S, MnO, $Fe_2O_{3(total)}$, MgO, ±CaO Zn, Pb, B
Quartz-muscovite	plagioclase, amphibole, pyroxene Mg-chlorite, garnets, chloritoid, clinozoisite, calcite, margarite, rutile-anatase, tourmaline, staurolite biotite, pyrrhotite, pyrite	Losses: Na_2O, CO_2, CaO, Ba gains: S, $Fe_2O_{3(total)}$, MnO, MgO, Zn, Cu, Pb B, As, Sn
(2) Hanging wall		
Quartz-biotite-rutile/titanite-pyrrhotite-pyrite	tourmaline, calcite, garnet, epidote, hornblende, chloritoid, muscovite chalcopyrite	Losses: MgO, ±SiO_2 gains: S, CO_2, $Fe_2O_{3(total)}$, K_2O, ±MnO, CaO, Na_2O Zn, Cu, B
B. 20 North lens: Lower levels		
(1) Quartz-muscovite-biotite-chlorite	epidote, clinozoïsite, allanite, rutile tourmaline, pyrite, carbonate	Losses: Na_2O, TiO_2 gains: MgO, S, CO_2, K_2O, $Fe_2O_{3(total)}$, MnO, B
(2) Quartz-garnet-muscovite-biotite	epidote, clinozoïsite, allanite, chlorite chloritoid, rutile-anatase, ilmenite, titanite, staurolite, tourmaline, kyanite carbonate	Losses: Na_2O, ±CO_2 gains: S, MnO, MgO, $Fe_2O_{3(total)}$, CaO ± K_2O
(3) Quartz-staurolite-muscovite-garnet ±biotite, pyrite	biotite, pyrite, albite, pyrophyllite, clinozoïsite, rutile/ilmenite, chlorite, margarite, garnet, sphalerite	Losses: Na_2O, CO_2, CaO, K_2O, ± SiO_2, Ba gains: S, MnO, $Fe_2O_{3(total)}$, MgO, Zn, Pb, B
(4) Quartz-muscovite-pyrite-paragonite±kyanite-andalusite	pyrophyllite, rutile, sphalerite, pyrrhotite chalcopyrite	Losses: CO_2, CaO Na_2O, MgO, MnO, SiO_2 gains: S, $Fe_2O_{3(total)}$, ±K_2O, Au, Zn, Cu, Pb, As
(5) Quartz-pyrite-kyanite-andalusite-chalcopyrite-gold	muscovite, paragonite, pyrophyllite sphalerite, pyrrhotite, ±arsenopyrite plagioclase, siderite, chloritoid, garnet	Losses: CaO, CO_2, Ba Na_2O, MnO, MgO, K_2O gains: S, $Fe_2O_{3(total)}$, TiO_2 Au, Cu, Ag, Zn, Pb, As Sb, Bi
(6) Quartz-kyanite-pyrite-andalusite	pyrophyllite, muscovite/paragonite rutile, staurolite, garnet, sphalerite, chalcopyrite	Losses: CO_2, Na_2O, CaO, K_2O, MgO, SiO_2, Ba gains: S, $Fe_2O_{3(total)}$, TiO_2 ± MnO, Zn, Cu, Au, Pb, As, Sn, B K_2O, Au, Zn

[1] Based on Tables 3 and 5 and Figures 7, 9, 10, and 14

basaltic andesite. The Zr-, TiO_2-, and Al_2O_3-bearing components of these rocks appear to have been unaffected by the alteration and metamorphism (Table 3, Fig. 7).

The quartz-garnet-biotite-muscovite footwall alteration of the 20 North lens is characterized by decrease in Na_2O as well as a very minor decrease in K_2O (Fig. 7) accompanied by a significant increase in MnO and locally in CaO and $Fe_2O_{3(total)}$ (total Fe reported as Fe_2O_3). MnO concentrations average 0.54 wt percent but are as high as 2.76 wt percent. These changes reflect the increase in abundance of pink garnet, with associated clinozoïsite and sulfide veinlets toward the massive sulfides. The Au, Ag, Cu, and Pb contents of the garnet-rich zone remain rather low, whereas the Zn content is relatively high. The thin quartz-muscovite-pyrite assemblage in the immediate footwall of the 20 North lens has slightly higher K_2O and S concentrations compared to the

quartz-garnet-biotite-muscovite assemblage, and lower MnO, CaO, and $Fe_2O_{3(total)}$ contents (Table 3). The quartz-muscovite-pyrite assemblage is also characterized by high concentrations of Zn, Cu, Pb, and Sn adjacent to the 20 North Au zone (Table 3).

The Ishikawa alteration index [AI = $100*(MgO + K_2O)/(MgO + K_2O + Na_2O + CaO)$: Ishikawa et al., 1976] and a chlorite-pyrite index [CPI = $100*(MgO + FeO_{(total)})/(MgO + FeO_{(total)} + Na_2O + K_2O)$] modified after Large et al. (2001), in the absence or only traces of carbonate, show some increase toward the ore zone (Fig. 7). However, most of the AI values in the footwall of the 20 North lens are below 50, despite the Na_2O depletion. This reflects the lack of significant K and Mg metasomatism in the footwall. At LaRonde Penna, sodium depletion is a better qualitative measure of the alteration intensity than the AI index. The alteration box plot of Large et
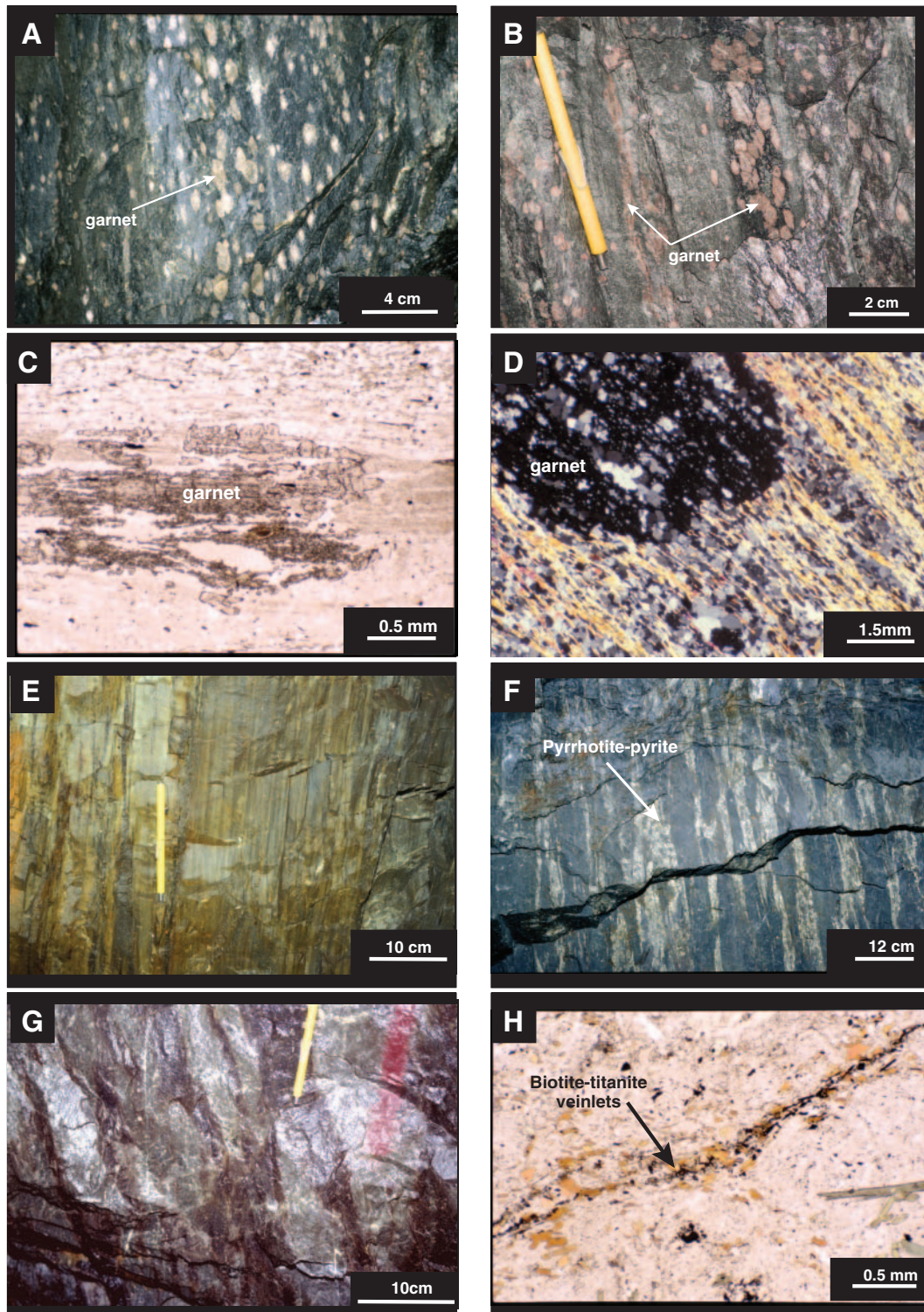
FIG. 5. A. Large pink garnets in black biotite-rich matrix in footwall of 20N Au zone (section view, stope 143-20-59). B. Elongated pink garnet porphyroblasts in a quartz-biotite-muscovite matrix, footwall of the 20N Au zone (section view, stope 137-20-62). C. Photomicrograph showing elongated syn- to late deformation Mn-rich garnet (plane-polarized light). D. Garnet porphyroblast, showing inclusions of quartz oriented parallel to the main foliation defined by muscovite and quartz in the rock matrix (cross-polarized light). E. Section view showing the quartz-muscovite alteration assemblage in the immediate footwall of the 20N Au zone (level 146, access drift). F. Pyrrhotite-pyrite stringers in basaltic andesite transposed parallel to the main foliation in the hanging wall of the 20N Zn zone (section view, level 146 access drift). G. Fracture-controlled pink alteration caused by disseminated titanite and rutile + anatase in hanging wall of the 20N Zn zone (level 146, access drift). H. Photomicrograph showing biotite-titanite trail within basaltic-andesite (5.4 unit), hanging wall of the 20N Zn zone (plane-polarized light).

TABLE 2. Microprobe Analyses of Garnet in the Footwall of 20 North Au

Sample no.	LABD-045-2000	LABD-234-2000	LAPL-86-2000	Average
Analyses (%)	5	4	2	11
SiO_2	36.85	38.13	37.28	37.42
TiO_2	0.17	0.05	0.19	0.14
Al_2O_3	20.81	20.69	20.82	20.77
FeO^*	27.22	30.33	13.75	23.77
MnO	9.46	5.86	16.27	10.53
MgO	0.51	1.47	0.07	0.68
CaO	5.06	3.97	10.69	6.58
Na_2O	0.03	0.05	0.01	0.03
K_2O	<0.01	<0.01	<0.01	<0.01
Cr_2O_3	0.02	0.00	<0.01	0.01
NiO	0.03	0.00	<0.01	0.02
V_2O_3	<0.01	0.03	<0.01	0.03
Total	100.16	100.57	99.13	99.95
Numbers of ions on the basis of 24 (O)				
Si	5.984	6.101	6.023	6.036
Al	0.016	0.000	0.000	0.005
Total	6.000	6.101	6.023	6.041
Al	3.968	3.906	3.964	3.946
Ti	0.021	0.005	0.023	0.016
Total	3.989	3.911	3.986	3.962
Mg	0.123	0.352	0.017	0.164
Fe^{2+*}	3.691	4.057	1.859	3.202
Mn	1.301	0.793	2.227	1.440
Na	0.008	0.015	0.000	0.008
Ca	0.880	0.680	1.851	1.137
Total	6.004	5.897	5.936	5.945

* Represents total iron content

al. (2001) for the 5.2 rhyodacite-rhyolite unit distinguishes the altered rocks from the least altered protolith (Fig. 8A). This trend is analogous to the chlorite ± muscovite ± pyrite alteration typical of VMS deposits (Large et al., 2001). Some of the least altered samples plot in the lower left corner, which is most probably related to low-temperature seawater "diagenesis" instead of ore-related hydrothermal alteration (cf. Large et al., 2001).

A more rigorous attempt to analyze the changes in volume and concentrations of the components in the altered rocks was performed using the best-fit isocon method (Grant, 1986). Based on field mapping, petrography, and lithogeochemistry, a group of 10 samples was selected from several hundred analyses to define the average composition of the least altered protolith. Al_2O_3 and Zr were used as the least mobile elements to define the best-fit isocon in plots of element concentrations in altered versus least altered samples. The isocon is a reference line that passes through the origin and which corresponds to zero concentration change. An isocon of slope 1 also coincides with the constant mass (Fig. 9A, B). The results for the quartz-garnet-biotite-muscovite assemblage indicate large gains in MnO, $Fe_2O_{3(total)}$, and MgO with minor gains of CaO and losses of Na_2O and K_2O, typical of alteration associated with VMS deposits (Franklin et al., 1981; Large et al., 2001). The isocon method also indicates gains in Au, Zn, Pb, and B, and losses in V and Ba (not shown). Compared to the least altered protolith, the quartz-muscovite assemblage shows elevated concentrations of $Fe_2O_{3(total)}$, MnO, MgO, S, Cu, Pb, Zn, Sn, Au, and B and lower concentrations of Na_2O, CaO, CO_2 and Ba (Table 3, Fig. 9B).

The pink quartz-rutile-titanite-biotite-chlorite assemblage in the hanging wall of the 20N Zn zone is characterized by high concentrations of Na_2O (up to 8 wt %). This may indicate that Na_2O leached from the footwall quartz-garnet-biotite-muscovite assemblage was added to rocks in the immediate hanging wall. A similar sodium enrichment in the hanging wall of VMS deposits has been described by Callaghan (2001) and Gemmell and Fulton (2001). However, elevated Na_2O concentrations in the hanging-wall lithologic units may simply reflect the original high concentration of Na_2O in the basaltic andesite (avg 5.15 wt %; Table 3) as suggested by Figure 9C. Such elevated Na_2O concentrations may be related to early Na metasomatism. The isocon for Al_2O_3, TiO_2, and Zr in the hanging-wall rocks diverges from the slope of 1 and suggests a slight mass and/or volume increase (Fig. 9C). $Fe_2O_{3(total)}$, S, and CO_2 were added to the rocks with a very slight increase in K_2O, MnO, CaO, and Na_2O and a small decrease in MgO and SiO_2 (Table 3, Fig. 9C). In terms of traces elements Cu, Zn, Pb, and B increase compared to the least altered basaltic andesite (Table 3). Overall, the hanging-wall rocks are not significantly chemically altered compared to the protolith. This may reflect the strong fracture-controlled nature of the alteration.

Deep levels of the 20 North lens

Mineralogy: At depth in the mine (≥1,900 m), the 20 North massive sulfides lens grades into a Au-rich aluminous replacement and stockwork zone. The transition from the alteration zones present in the upper levels of the mine to the aluminous zone is gradual, and staurolite, andalusite, and kyanite first appear on level 191 (1,910 m below surface). Although base metal concentrations are lower, Zn is enriched toward the upper part of the lens (Fig. 10). As originally described for Bousquet 1 (Valliant et al., 1983), the aluminous zone at LaRonde Penna is characterized by an intense acid leaching, but in contrast to Bousquet 1, hosts significant Au. The Zr (170–200 ppm) and TiO_2 (0.5–0.6 wt %) content of the inferred protolith is identical to the unit 5.2b rhyodacite-rhyolite in the footwall of the 20 North lens (Fig. 10). However, in contrast to the upper part of the deposit, here the basaltic andesite (unit 5.4) is absent in the stratigraphic hanging wall, and only the rhyodacitic to rhyolitic volcanic flow breccia (unit 5.5) are present (Fig. 3).

A number of different alteration facies are recognized over several tens to a few hundreds of meters in the core of the aluminous zone. As ore is approached these are (1) quartz-muscovite-biotite-chlorite, (2) quartz-garnet-muscovite-biotite-chlorite, (3) quartz-staurolite-muscovite-garnet ± biotite ± pyrite, (4) quartz-muscovite-paragonite-pyrite ± kyanite-andalusite, (5) quartz-pyrite-kyanite-andalusite-chalcopyrite-gold , and (6) quartz-kyanite-andalusite-sphalerite. The first four facies form the envelope of the ore zone and may be present in both the footwall and hanging wall (Fig. 11). The last two coincide with the ore zones. The thickness of each of these facies is highly variable (from centimeters to tens of meters) and they are not always all present, but where present they occur in the order depicted in Figure 11.
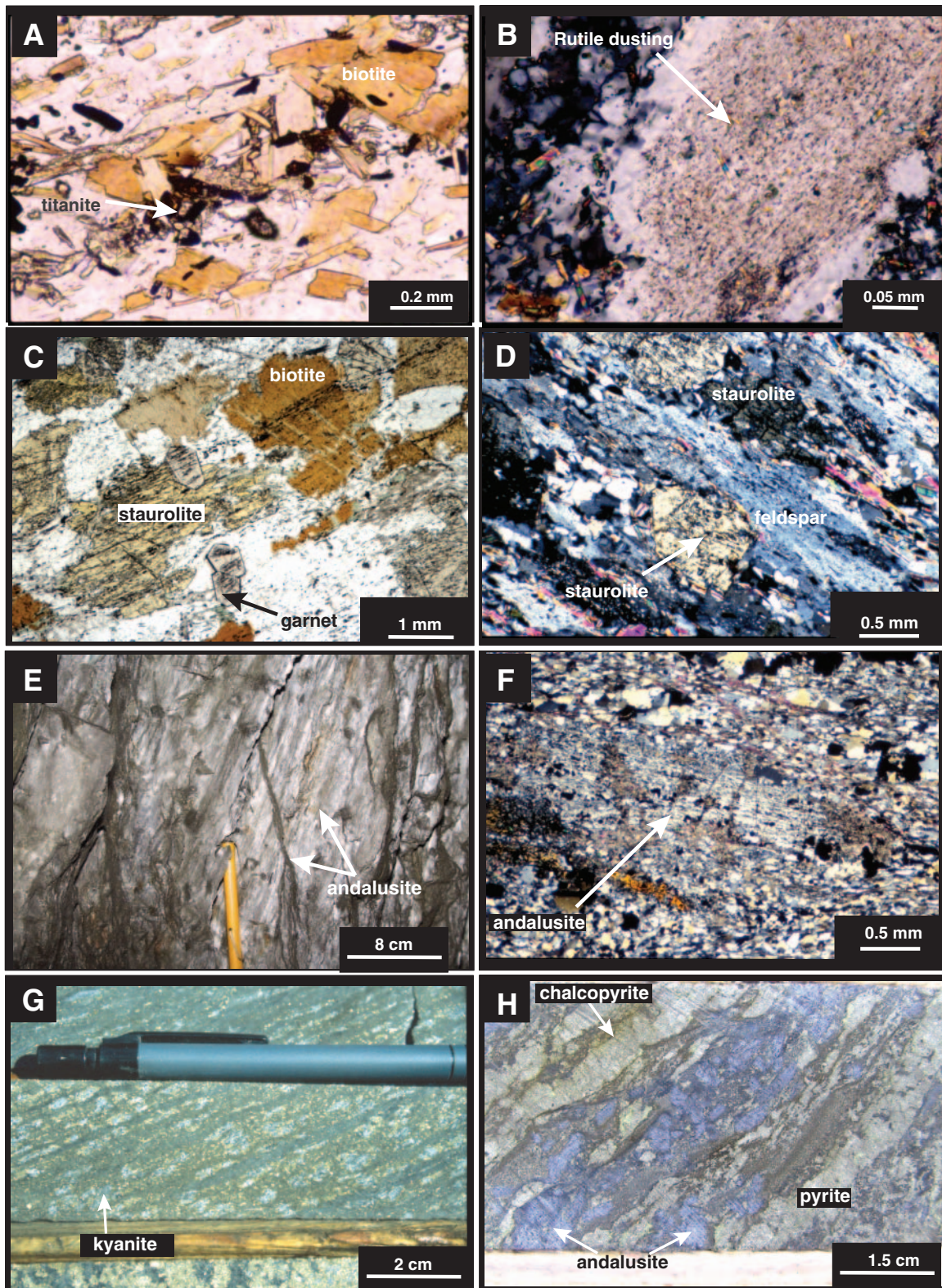
FIG. 6. A. Close-up of Figure 5H. B. Photomicrograph showing fine rutile dusting within a feldspar microphenocryst (cross-polarized light). C. Photomicrograph showing the quartz-biotite-staurolite-garnet assemblage (cross-polarized light). D. Photomicrograph showing elongated syndeformation feldspar porphyroblast with staurolite (cross-polarized light). E. Large andalusite porphyroblast in quartz-muscovite-andalusite schist (section view, stope 215-20-46). F. Photomicrograph showing elongated syndeformation andalusite porphyroblast (cross-polarized light). G. Typical drill core samples of highly strained, banded quartz-kyanite-pyrite auriferous replacement zone hosted by the rhyodacite-rhyolite (unit 5.2b). H. Typical drill core sample of deformed quartz-pyrite-kyanite-andalusite-chalcopyrite ore zone.

TABLE 3. Average Composition of Alteration Facies in the Footwall and Hanging Wall of the 20 North Lens, Upper and Intermediate Levels of the LaRonde Penna Deposit

| | Footwall 20 North lens | | | | | | | | | Hanging wall 20 North lens | | | | | |
| | Rhyodacite-rhyolite least altered 5.2b | | | qtz-grt-bio-mus | | | qtz-mus | | | Basaltic andesite least altered 5.4 | | | bio-rut/tit-po-py | | |
(%)	Average	STD	No.	Average	STD	No.	Average	STD	No.	Average	STD	No.	Average	STD	No.
SiO_2	73.30	2.48	10	68.33	4.28	37	69.41	4.86	13	56.83	4.08	8	49.67	6.82	22
TiO_2	0.48	0.17	10	0.66	0.06	37	0.64	0.08	13	1.11	0.12	8	0.99	0.23	22
Al_2O_3	13.94	0.85	10	13.36	0.88	37	13.86	1.30	13	20.36	1.23	8	18.70	3.38	22
$Fe_2O_{3(total)}$	2.00	1.10	10	7.16	3.84	37	6.58	3.68	13	4.68	2.43	8	10.81	6.33	22
MnO	0.06	0.03	10	0.54	0.55	37	0.11	0.13	13	0.07	0.03	8	0.07	0.04	22
MgO	0.49	0.24	10	1.24	0.44	37	0.81	0.51	13	3.14	1.24	8	2.40	0.93	22
CaO	1.65	0.45	10	2.94	1.46	37	1.34	1.18	13	5.10	2.17	8	5.44	2.54	22
Na_2O	4.94	1.18	10	1.83	1.25	37	1.41	0.56	13	5.15	1.16	8	5.06	1.38	22
K_2O	2.09	1.05	10	1.80	0.57	37	2.15	0.85	13	1.12	0.64	8	1.38	0.61	22
P_2O_5	0.10	0.05	10	0.13	0.02	37	0.09	0.05	13	0.12	0.02	8	0.11	0.04	22
LOI	1.08	0.62	10	1.68	0.79	37	3.19	1.46	13	1.84	0.65	8	5.03	4.02	22
Total (%)	100.14	1.56	10	99.51	0.83	37	99.43	0.90	13	99.72	0.65	8	100.14	0.89	22
S (%)	0.07	0.08	10	0.51	1.09	37	2.81	2.46	13	0.80	0.70	8	5.49	4.87	22
CO_2 (%)	0.46	0.44	10	0.39	0.40	37	0.05	0.08	13	0.16	0.28	8	1.13	1.86	22
AI	28.54	13.95	10	41.33	15.35	37	53.90	18.12	13	29.46	6.83	8	26.96	8.25	22
CCPI	25.14	10.61	10	67.33	15.87	37	63.29	16.67	13	53.20	10.60	8	63.51	14.16	22
Metals (ppm)															
Au (ppb)	2	1	10	11	19	37	16	18	13	5	7	8	16	20	23
Cu	11	10	10	28	86	37	184	371	13	93	24	8	145	160	23
Ag	b.d.	b.d.	10	1	2	37	2	3	13	1	1	8	2	2	23
Zn	39	23	10	1731	4148	37	1093	1747	13	62	31	8	334	410	23
Pb	2	1	10	128	502	37	221	527	13	23	54	8	40	106	23
As	3	3	10	10	b.d.	24	19	22	10	9	3	6	15	14	14
Sb	4	2	10	1	2	24	3	2	10	2	2	6	2	2	14
Sn	9	2	9	15	30	37	92	149	13	109	287	8	81	197	23
Trace elements (ppm)															
V	27	21	10	16	8	34	24	25	9	305	22	7	271	44	19
Ba	503	245	10	310	142	34	178	70	9	282	98	7	239	123	19
Cr	3	1	10	10	17	37	9	15	13	91	21	8	101	32	23
Mn	411	206	9	3485	3570	34	629	727	9	454	214	7	538	247	19
B	5	b.d.	2	948	3216	24	464	913	10	137	82	6	237	250	14
Bi	4	1	9	5	4	37	9	9	13	44	115	8	47	107	23
Y	28	8	10	38	6	37	34	6	13	12	3	8	10	4	23
Zr	189	20	10	192	14	37	204	19	13	51	20	8	48	22	23

Notes: SiO_2, TiO_2, Al_2O_3, $Fe_2O_3{}^T$, MnO, MgO, CaO, Na_2O, K_2O, P_2O_5, LOI, Y, Zr = ICP-AES (INRS), Ag, Cu, Zn, Pb, Sn, V, Ba, Cr, Mn, Bi = ICP-80 (XRAL), Au (ppb) = Fire Assay (XRAL), As, Sb = Fusion/ICP/Hybride AA (XRAL), S = Leco (XRAL), CO_2 = Coulometry (XRAL), B = ICP90A (XRAL), bio = biotite, grt = garnet, mus = muscovite, po = pyrrhotite, py = pyrite, qtz = quartz, rut = rutile, tit = titanite, STD = standard deviation, No. = number of analyses, AI = Alteration Index (Ishikawa et al., 1976), CCPI = chlorite-carbonate-pyrite alteration index (Large et al., 2001), b.d. = below detection
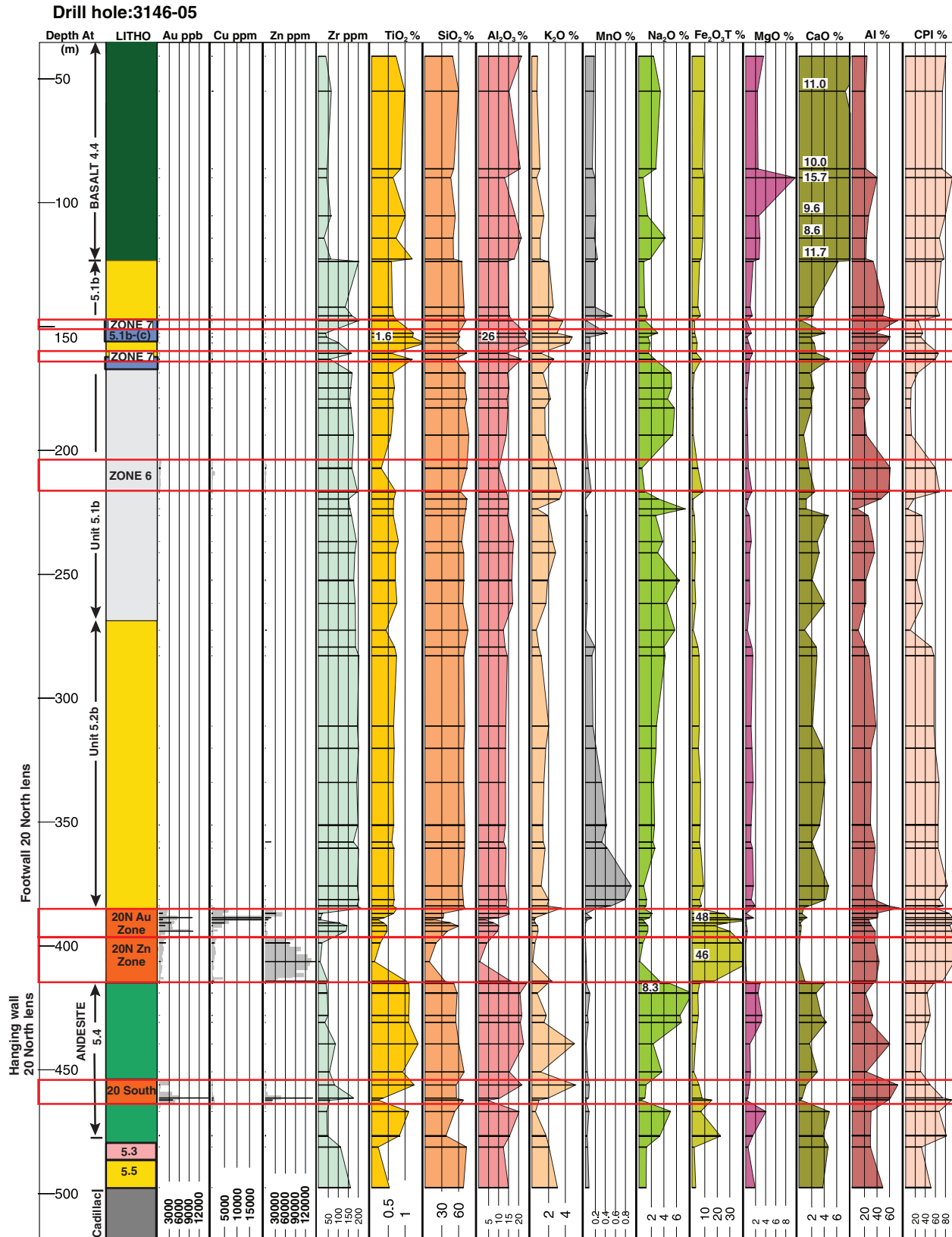
FIG. 7. Geochemical profile of drill hole 3146-05 (shown in Fig. 2). Locations of analyzed samples and results are indicated by short horizontal lines. Gray bars in Au, Cu, and Zn columns represent assays obtained by Agnico-Eagle Mines Ltd. Number in profile indicates out of scale result. AI = alteration index (Ishikawa et al., 1976), CPI = chlorite-pyrite index (modified from Large et al., 2001).
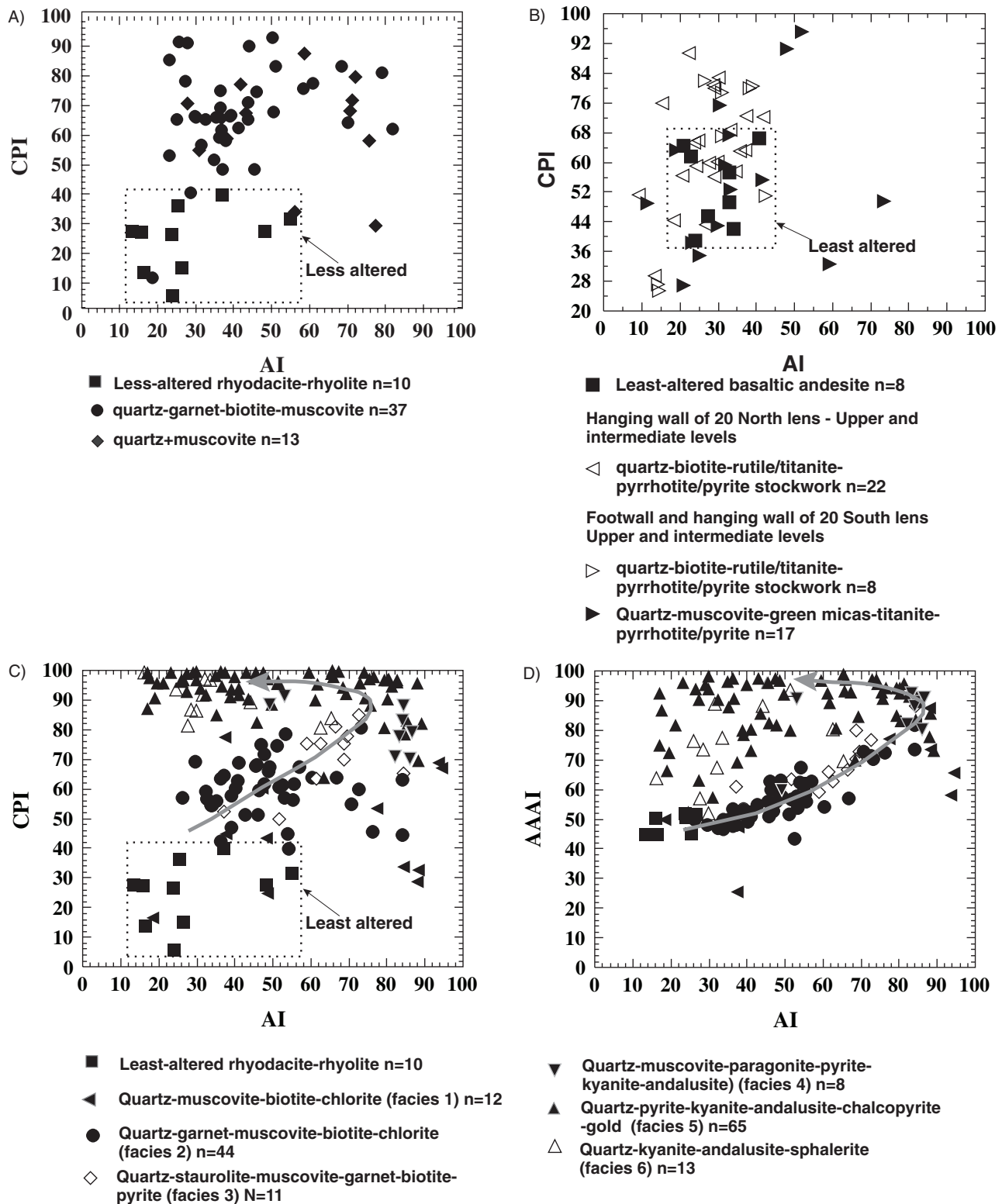
FIG. 8. Box plot diagrams (Large et al., 2001). A. Alteration of the 20 North lens footwall rhyodacite-rhyolite (unit 5.2b) in upper to intermediate levels of the mine. B. Alteration of basaltic andesite (unit 5.4) in the hanging wall of lens 20 North and hanging wall and footwall of lens 20 South, in the upper to intermediate levels of the mine. C. Aluminous alteration of the 20 North lens footwall rhyodacite-rhyolite (unit 5.2b), lower levels of the mine. D. Modified box plot diagram using the advanced argillic alteration index (AAAI) of Williams and Davidson (2004), showing aluminous alteration of the 20 North lens footwall rhyodacite-rhyolite (unit 5.2b), lower levels of the mine. AI = alteration index (Ishikawa et al., 1976), CPI = chlorite-pyrite index (modified from Large et al., 2001), AAAI = advanced argillic alteration index (Williams and Davidson, 2004). Note that the symbols and related assemblages for (C) and (D) pertain to both plots.

A) Footwall of the 20 North lens
quartz-garnet-biotite-muscovite assemblage

B) Footwall of the 20 North lens
quartz-muscovite assemblage

C) Hanging-wall of the 20 North lens:
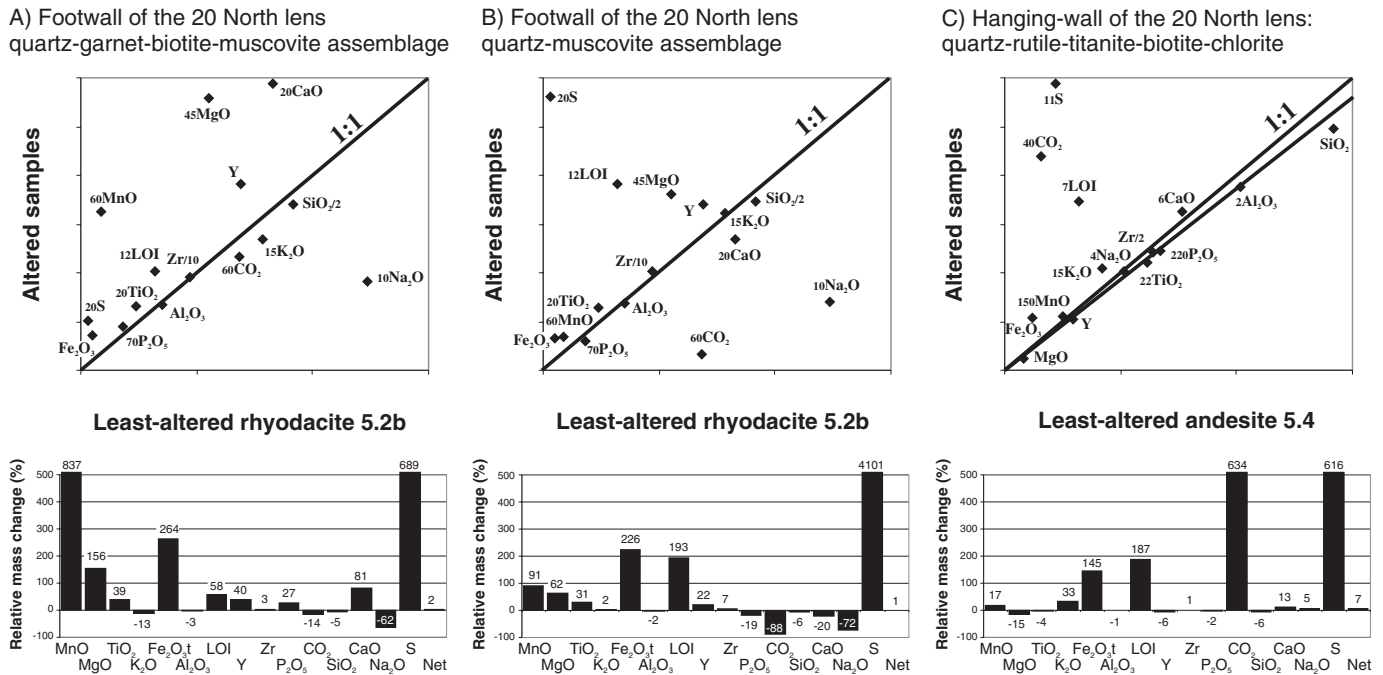quartz-rutile-titanite-biotite-chlorite

FIG. 9. Best-fit isocon diagram (Grant, 1986) with the relative mass gains and losses for the major elements quantified using equations given in Grant (1986) and the method proposed by Huston (1993), showing the relative mass change in wt percent. Average major and minor components are plotted as wt percent of the oxides. Data for trace elements are plotted in 0.1 ppm. As suggested in Grant (1986), components are scaled for a clearer view and to show changes in components that might be considered minor relative to silica or alumina but which are useful alteration parameters. A. Quartz-garnet-biotite-muscovite assemblage hosted by the 20N Au zone footwall rhyodacite-rhyolite (unit 5.2b), upper and intermediate levels of the mine. B. Quartz-muscovite alteration facies hosted by the 20N Au zone footwall rhyodacite-rhyolite (unit 5.2b), upper and intermediate levels of the mine. C. Quartz-biotite-rultile-titanite assemblage hosted by basaltic andesite (unit 5.4) in the hanging wall of lens 20N Zn zone, upper and intermediate levels of the mine.

The quartz-muscovite-biotite-chlorite assemblage (1) is the most distal. It is up to a few hundred meters wide. It forms an outer zone mainly composed of quartz (≤60%), muscovite (≤65%), biotite (≤25%), and Mg chlorite (≤15%), with minor amounts of others minerals listed in Table 1. Biotite is locally replaced by Mg chlorite and the TiO$_2$ liberated during the process forms rutile-anatase. Muscovite is oriented parallel to the main foliation and its proportion increases toward the mineralized zones.

The quartz-garnet-muscovite-biotite-chlorite assemblage (2) is up to several tens of meters thick both in the footwall and hanging wall. In some sections, it is particularly wide in the hanging wall of the 20 North lens (Fig. 3). It is characterized by pink-colored subhedral garnet poikiloblasts (1–6 mm, 3–20 vol %) and by metasomatic and/or metamorphic layering with muscovite-rich bands (≤2–4 cm wide) alternating with quartz-rich or dark gray-colored garnet-biotite-epidote-rich bands oriented subparallel to the main foliation. Garnet is syn- to late deformation. It is very similar to garnet in the quartz-garnet-biotite-muscovite assemblage present in the footwall of the 20N Au zone in the upper levels of the mine. Biotite is also aligned parallel to the main foliation, and it is locally replaced by muscovite or by chlorite with rutile. Locally, Mg chlorite, rutile-anatase-clinozoïsite veinlets are present (Table 1). Traces to minor amounts of other minerals are commonly present (Table 1) with up to 8 vol percent pyrite and traces of sphalerite, pyrrhotite, and chalcopyrite.

The quartz-staurolite-muscovite-garnet ± biotite ± pyrite assemblage (3) is closer to the mineralized zone. It is centimeters to a few meters wide and, where present, is especially well developed in the footwall of the ore zone. The presence of staurolite constitutes the first evidence of aluminous alteration (Fig. 6C). Staurolite forms yellowish, syn- to late deformation porphyroblasts (1–4 mm, 3–20 vol %) containing up to 6.9 percent ZnO (Table 4). The entire assemblage is characterized by elevated Zn concentrations, probably due to the presence of zincian staurolite and disseminated sphalerite (Table 5). Staurolite is commonly concentrated in 3- to 5-mm-wide foliation-parallel layers with muscovite, albite, quartz, and traces of garnet (Fig. 6C). The staurolite is locally replaced by muscovite and/or pyrophyllite. Albite also forms porphyroblasts aligned parallel to the main foliation and concentrated in (≤3–5 mm) layers (Fig. 6D). Albite is replaced by muscovite, clinozoïsite, and quartz and is locally dusted by rutile and/or ilmenite.

The quartz-muscovite-paragonite-pyrite ± kyanite-andalusite assemblage (4) is adjacent to the ore and is anomalous in Au to weakly mineralized (≤1–2 g/t Au). This alteration zone is generally centimeters to meters wide, strongly altered, and characterized by the presence of kyanite (≤7 vol %) and locally andalusite (≤5 vol %) with quartz (≤60 vol %), muscovite (≤30 vol %), paragonite (≤60 vol %), pyrophyllite (≤12 vol %), and rutile (≤2 vol %). Due to intense deformation, the assemblage forms a banded schist with millimeter-
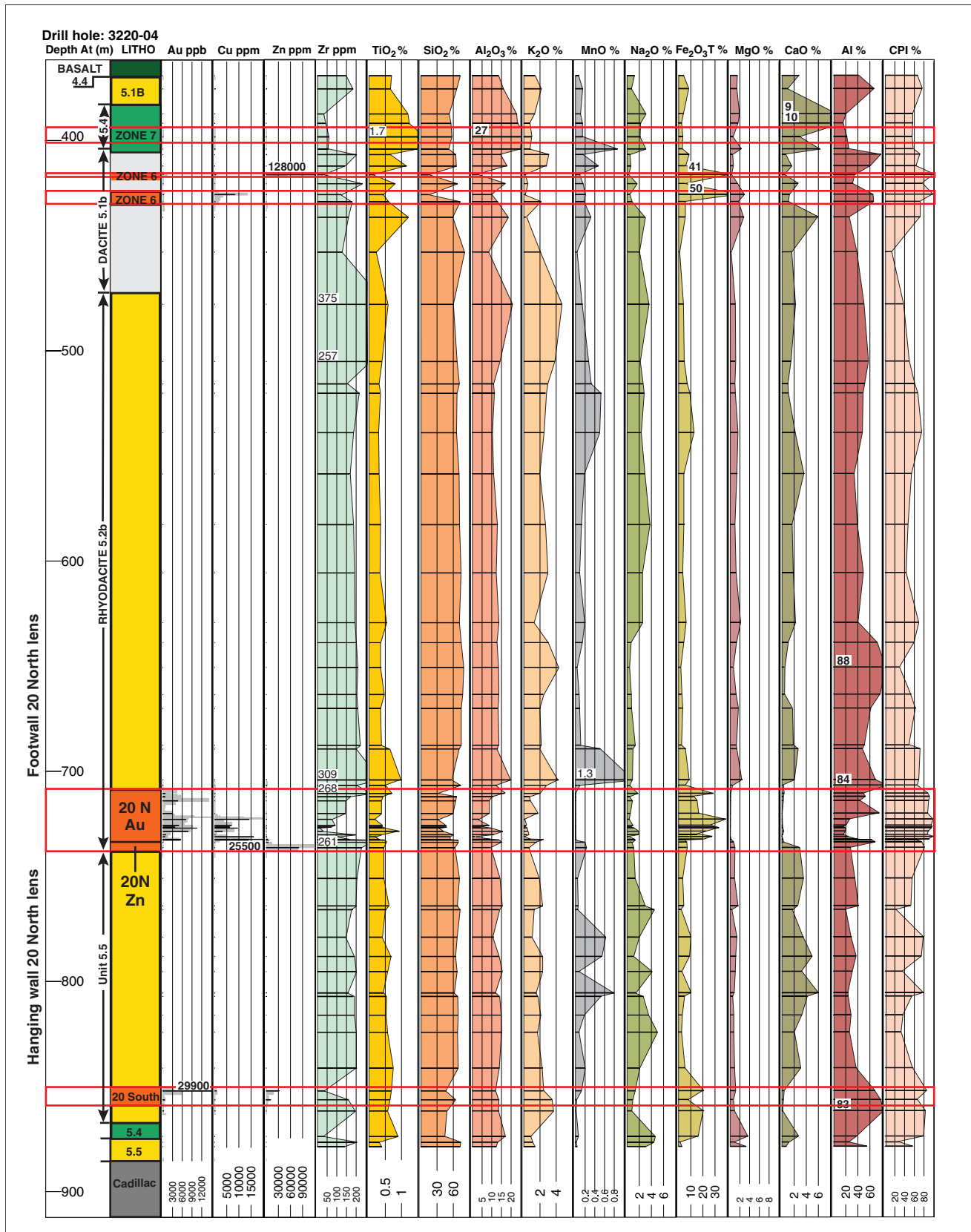
FIG. 10. Geochemical profile of drill hole 3220-04 (shown in Fig. 3). Locations of analyzed samples and results are indicated by short horizontal lines. Number in profile indicates out of scale result. AI = alteration index (Ishikawa et al., 1976), CPI = chlorite-pyrite index (modified from Large et al., 2001).
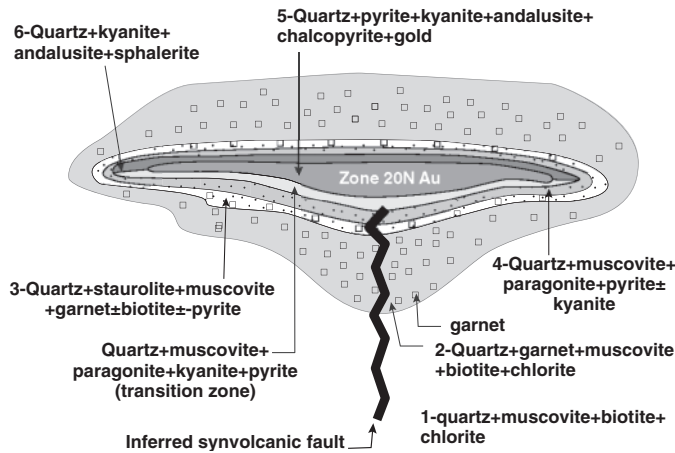
FIG. 11. Schematic representation of the distribution of the alteration assemblages in the lower part of the LaRonde Penna deposit.

wide quartz-pyrite bands alternating with muscovite-paragonite–rich bands. Pyrite is more abundant (5–30 vol %) and coarser grained than in assemblage (3). Pyrite, kyanite, and andalusite increase in abundance toward the ore zone. Kyanite (≤3 mm) and andalusite form porphyroblasts dusted by fine pyrite and ilmenite and/or rutile and partly to strongly replaced by pyrophyllite. Andalusite commonly constitutes large, syn- to late main deformation porphyroblasts (≤1–2 cm) (Fig. 6E). The andalusite porphyroblasts are commonly elongated parallel to the main foliation and contain numerous

quartz inclusion trails also aligned parallel to the foliation (Fig. 6F). Biotite is entirely replaced (retrograded) by muscovite. There are also traces of sulfides (Table 1).

The quartz-pyrite-kyanite-andalusite-chalcopyrite-gold assemblage (5) is a highly strained ribboned replacement zone with sulfide stringers transposed by the main foliation and hosted by the rhyodacite-rhyolite unit (unit 5.2b, Fig. 6G, H). It hosts the ore and represents the extension of the 20 North lens at depth. The zone is up to 30 meters wide. The assemblage is dominated by quartz (≤65 vol %), pyrite (≤85 vol %), and kyanite (≤30 vol %) with variable proportions of andalusite (≤10 vol %), muscovite and/or paragonite and pyrophyllite (≤20 vol %), and other minerals as traces (Table 1). The sulfides are dominated by pyrite with variable proportions of chalcopyrite (≤17 vol %), sphalerite (≤1–3 vol %), pyrrhotite (≤1–4 vol %), and traces of arsenopyrite (Table 1). Gold grade varies within this assemblage, with the highest values being commonly associated with centimeter- to locally meter-wide bands of semimassive to massive coarse pyrite in a quartz-kyanite ± andalusite matrix devoid of muscovite and/or paragonite. Kyanite forms disseminated porphyroblasts (≤1.5 cm; Fig. 12A) or is concentrated in centimeter-wide foliation-parallel bands with quartz, andalusite, and pyrite. In the auriferous ore zone, the kyanite contains pyrite and/or chalcopyrite as disseminations or along the cleavages (Fig. 12B). Kyanite is commonly replaced by pyrophyllite or quartz (Fig. 12C). Andalusite constitutes large (≤1.5 cm) syn- to late deformation porphyroblasts elongated parallel to the main foliation and dusted by fine pyrite, chalcopyrite, quartz,

TABLE 4. Microprobe Analyses of Zn-Rich Staurolite, LaRonde Penna Mine

Element (%)	LABD-377-2000	LABD-377-2000	LABD-377-2000	LABD-377-2000	2002-083-stau39	2002-083-stau40
SiO_2	26.46	26.74	26.87	26.69	27.37	27.74
TiO_2	0.52	0.48	0.46	0.44	0.57	0.44
AL_2O_3	54.37	54.24	53.35	54.13	54.24	53.79
MgO	0.91	0.86	1.17	0.82	0.60	0.39
CaO	<0.01	<0.01	<0.01	<0.01	<0.01	<0.01
MnO	0.49	0.47	0.51	0.42	0.37	0.33
FeO	9.99	10.12	9.31	9.38	8.70	8.20
ZnO	5.00	5.23	6.37	6.88	6.80	6.88
Na_2O	0.06	0.04	0.08	0.09	0.08	0.11
K_2O	<0.01	<0.01	0.01	0.01	<0.01	<0.01
H_2O	2.13	2.14	2.13	2.14	2.15	2.14
Total	99.91	100.31	100.27	101.00	100.87	100.01
Numbers of ions on the basis of 23 (O, OH)						
SiO_2	3.718	3.748	3.678	3.736	3.813	3.887
AL_2O_3	9.004	8.959	8.845	8.929	8.908	8.884
TiO_2	0.054	0.500	0.049	0.046	0.059	0.046
Total	9.058	9.459	8.894	8.975	8.967	8.930
MgO	0.191	0.179	0.246	0.171	0.125	0.080
FeO	1.174	1.185	1.095	1.098	1.014	0.961
ZnO	0.518	0.541	0.662	0.711	0.700	0.712
MnO	0.058	0.055	0.060	0.050	0.043	0.039
CaO	0.000	0.000	0.000	0.000	0.000	0.000
Total	1.941	1.960	2.063	2.030	1.882	1.792
Na_2O	0.016	0.011	0.021	0.025	0.021	0.029
K_2O	0.000	0.000	0.003	0.002	0.000	0.000
H_2O	0.008	0.008	0.008	0.008	4.046	4.046
Total	0.016	0.019	0.032	0.035	4.067	4.075

TABLE 5. Average Composition of Alteration Facies in the Footwall and Hanging Wall of the 20 North Lens, Lower Levels of the LaRonde Penna Mine

Alteration	rhyodacite-rhyolite			1-qtz-mus-bio-chl least altered 5.2b			2-qtz-grt-mus-bio			3-qtz-sta-grt-ser			4-qtz-mus-py-par-kya			5-qtz-py-kya-cpy-gold			6-qtz-kya-py-and-sp		
(%)	Average	STD	No.	Average	STD	No.	Average	STD	No.	Average	STD	No.	Average	STD	No.	Average	STD	No.	Average	STD	No.
SiO_2	73.30	2.48	10	73.01	5.13	12	70.61	2.70	44	70.80	3.75	11	60.69	12.15	8	50.05	17.57	65	43.26	20.50	13
TiO_2	0.48	0.17	10	0.39	0.09	12	0.52	0.16	44	0.56	0.15	11	0.52	0.12	8	0.42	0.15	65	0.53	0.12	13
Al_2O_3	13.94	0.85	10	12.99	1.30	12	12.99	1.28	44	13.55	0.88	11	12.21	2.63	8	9.72	3.85	65	10.75	4.13	13
$Fe_2O_{3(total)}$	2.00	1.10	10	2.52	1.13	12	5.24	2.09	44	6.13	2.33	11	14.13	6.83	8	24.18	12.35	65	19.84	11.95	13
MnO	0.06	0.03	10	0.07	0.09	12	0.29	0.29	44	0.23	0.23	11	0.04	0.08	8	0.01	0.04	65	0.05	0.06	13
MgO	0.49	0.24	10	1.94	1.69	12	1.44	0.53	44	1.27	0.46	11	0.29	0.33	8	0.09	0.23	65	0.29	0.54	13
CaO	1.65	0.45	10	1.69	3.07	12	2.29	1.03	44	0.92	0.60	11	0.18	0.10	8	0.10	0.08	65	0.38	0.75	13
Na_2O	4.94	1.18	10	1.79	1.92	12	1.89	1.03	44	1.02	0.62	11	0.59	0.47	8	0.50	0.48	65	1.01	0.69	13
K_2O	2.09	1.05	10	3.05	1.64	12	2.36	0.75	44	1.88	0.48	11	2.41	0.86	8	0.82	0.90	65	0.57	0.37	13
P_2O_5	0.10	0.05	10	0.07	0.03	12	0.10	0.04	44	0.10	0.04	11	0.09	0.02	8	0.05	0.04	65	0.06	0.07	13
LOI	1.08	0.62	10	2.32	1.86	12	1.77	0.78	44	2.86	1.16	11	8.32	3.85	8	12.80	6.45	65	12.40	6.38	13
Total (%)	100.14	1.56	10	99.93	1.45	12	99.66	1.00	44	100.16	1.09	11	99.74	0.61	8	99.26	1.76	65	93.56	13.54	13
S (%)	0.07	0.08	10	0.22	0.54	12	0.38	0.83	44	2.28	1.80	11	10.48	5.70	8	19.26	10.45	65	17.17	12.58	13
CO_2 (%)	0.46	0.44	10	0.66	1.94	12	0.39	0.49	44	0.06	0.09	11	0.01	0.01	8	0.01	0.01	65	0.02	0.03	13
AI	28.54	13.95	10	63.65	26.63	12	49.10	14.29	44	63.80	12.21	11	76.05	15.52	8	53.50	22.59	65	36.41	15.04	13
CCPI	25.14	10.61	10	45.98	19.48	12	60.10	9.37	44	70.04	11.30	11	81.20	8.13	8	93.28	7.31	65	90.63	6.40	13
AAAI	51.36	5.99	9	61.89	17.13	12	56.67	8.64	44	69.69	8.93	11	84.33	10.78	8	87.66	9.65	65	72.29	13.68	13
Metals (ppm)																					
Au (ppb)	2	1	10	6	6	12	10	24	44	47	47	11	578	248	8	5218	5915	65	1120	1860	13
Cu	11	10	10	10	12	12	12	11	44	31	42	11	93	96	8	5441	9808	65	5260	17953	13
Ag	b.d.	b.d.	10	b.d.	b.d.	12	1	1	44	1	1	11	2	1	8	12	31	65	16	20	13
Zn	39	23	10	41	34	12	165	254	44	759	1486	11	117	88	8	1177	4281	65	75832	96857	13
Pb	2	1	10	5	5	12	29	101	44	37	34	11	68	46	8	97	90	65	706	1016	13
As	3	3	10	10	b.d.	7	6	4	39	12	5	11	70	59	5	169	236	49	125	249	13
Sb	4	2	10	1	2	7	b.d.	b.d.	39	1	1	11	1	1	5	14	40	49	11	13	13
Sn	9	2	9	39	108	12	6	2	27	5	b.d.	9	7	3	7	23	35	65	152	283	7
Trace elements (ppm)																					
V	27	21	10	18	18	11	13	6	44	14	7	11	13	6	8	29	32	59	72	77	9
Ba	503	245	10	345	157	11	424	143	44	297	122	11	253	192	8	105	132	59	91	43	9
Cr	3	1	10	5	6	12	8	12	44	17	22	11	12	15	8	25	26	65	49	49	13
Mn	411	206	9	454	527	11	2102	1620	27	696	337	9	324	651	7	82	262	59	635	589	5
B	5	b.d.	2	56	68	7	29	41	39	26	21	11	39	31	5	35	47	49	242	750	13
Bi	4	1	9	4	2	12	3	1	27	3	b.d.	9	18	22	7	31	82	65	19	21	7
Y	28	8	10	35	8	12	42	7	44	38	4	11	30	10	8	17	11	65	15	14	13
Zr	189	20	10	203	20	12	203	18	44	213	19	11	202	42	8	144	66	65	125	94	13

Notes: SiO_2, TiO_2, Al_2O_3, $Fe_2O_3^T$, MnO, MgO, CaO, Na_2O, K_2O, P_2O_5, LOI, Y, Zr = ICP-AES (INRS), Ag, Cu, Zn, Pb, Sn, V, Ba, Cr, Mn, Bi = ICP-80 (XRAL), As, Sb = Fusion/ICP/Hybride AA (XRAL), S = Leco (XRAL), CO2 = Coulometry (XRAL), B = ICP90A (XRAL), and = andalusite, bio = biotite, chl = chlorite, cpy = chalcopyrite, grt = garnet, mus = muscovite, mv = green micas, par = paragonite, po = pyrrhotite, py = pyrite, qtz = quartz, rut = rutile, sp = sphalerite, sta = staurolite, tit = titanite, STD = standard deviation, No. = number of analyses, AI = Alteration Index (Ishikawa et al., 1976), CCPI = chlorite-carbonate-pyrite alteration Index (Large et al., 2001), AAAI = Advanced argillic alteration index (Williams and Davidson, 2004), b.d. = below detection
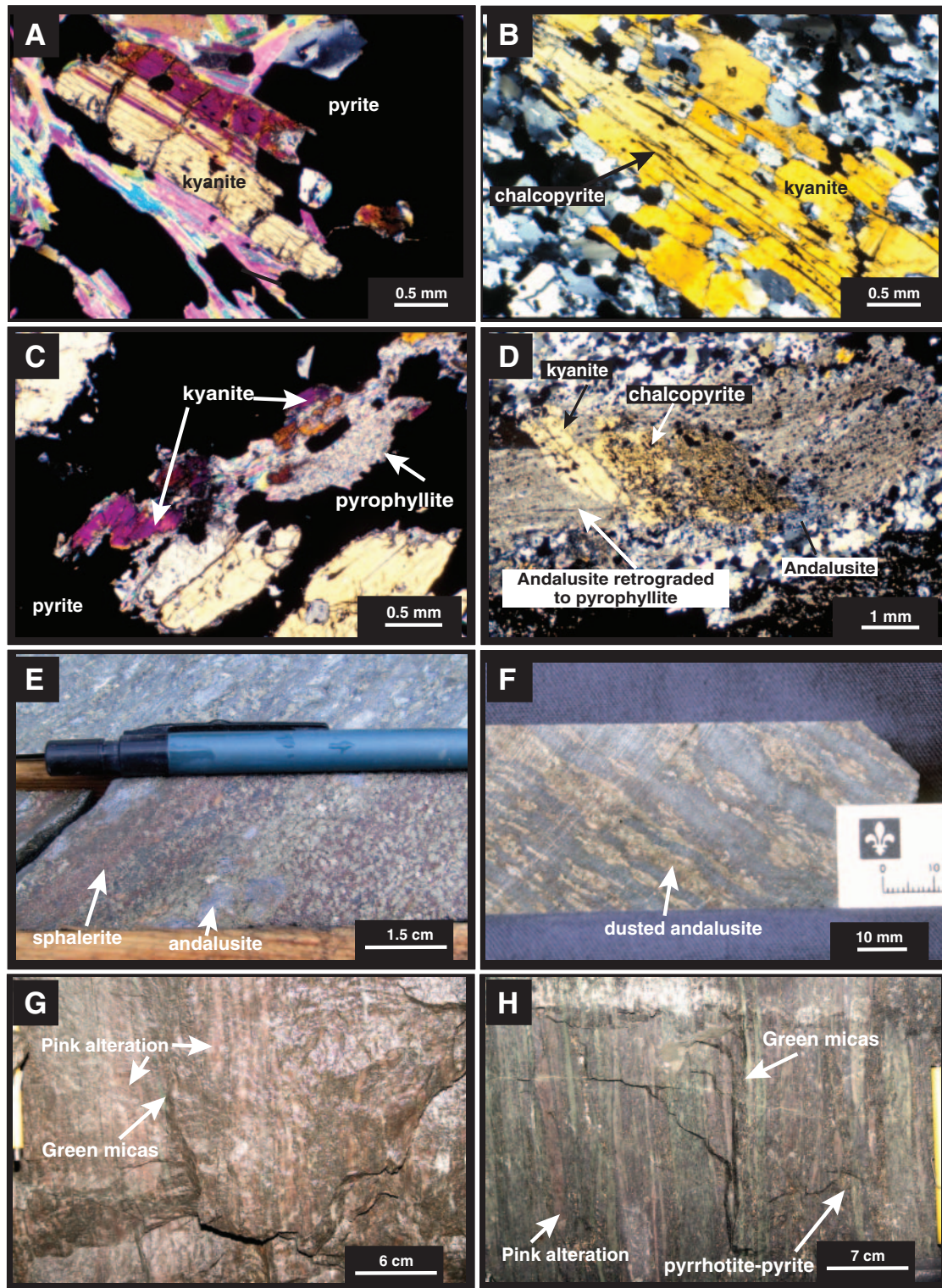
FIG. 12. A. Photomicrograph showing kyanite porphyroblast in a pyrite and muscovite matrix (cross-polarized light). B. Photomicrograph showing chalcopyrite within cleavages of kyanite prophyroblast (cross-polarized light). C. Photomicrograph showing kyanite porphyroblast partly retrograded to pyrophyllite (cross-polarized light). D. Photomicrograph of large syn-deformation andalusite porphyroblast retrograded to pyrophyllite and hosting an inclusion of an unoriented kyanite porphyroblast at a high angle to the foliation. The kyanite contains numerous fine chalcopyrite inclusions (cross-polarized light). E. Drill core sample of 20N Zn zone at depth in the mine showing recrystallized pyrite with andalusite in a matrix of sphalerite. F. Drill core sample of andalusite dusted by fine sphalerite. G. Pink quartz-biotite-rutile-titanite assemblage in footwall of lens 20 South (section view, stope 106-21-71). H. Strongly foliated alteration zone, showing alternating pink and green quartz-muscovite-green mica-titanite bands (section view, stope 106-21-80).

and rutile. As originally reported at Bousquet 1 (Valliant et al., 1983) and Bousquet 2-Dumagami (Marquis et al. 1990c; Tourigny et al., 1993; Teasdale et al., 1996), andalusite is commonly retrograded to pyrophyllite and may contain unoriented late to postdeformation kyanite (Fig. 12D). This alteration facies is analogous to the metamorphosed advanced argillic alteration described by previous authors working in the district and elsewhere by Ririe (1990).

The quartz-kyanite-andalusite-sphalerite assemblage (6) varies from several centimeters to 15 m thick and is distinguished by the abundance of sphalerite. Sphalerite is concentrated in massive to semimassive breccia layers (up to 15 cm thick) with pyrite and gangue clasts (Fig. 12E). Sphalerite has partly replaced or is present as a fine dusting of inclusions within kyanite and andalusite, yielding an orange-reddish color (Fig. 12F). Sphalerite also fills fractures and cleavages in kyanite. Pyrite (≤10 vol %) and chalcopyrite (traces) are significantly less abundant than in the gold-bearing alteration assemblage (facies 5). Kyanite in this assemblage forms aggregates of porphyroblasts associated with sphalerite in bands (≤1 cm) subparallel to the main foliation. Kyanite and andalusite are strongly replaced (retrograded) by pyrophyllite. Minor muscovite and/or paragonite and rutile are also present along with staurolite and garnet away from the ore zone (Table 1). Gold grades are uneconomic and commonly only anomalous, whereas Zn grades can reach up to 20 wt percent. This Zn-rich zone is the downdip equivalent to the massive sulfide of the 20N Zn zone in the upper part of the mine and typifies the Zn-rich enrichment toward the south-southeast evident in all sulfide lenses within the district.

Lithogeochemistry: Table 5 and Figure 10 show the geochemical chracteristics of mineralogical assemblages described above relative to the average composition of the precursor rhyodacite-rhyolite (unit 5.2b). The drill hole 3220-04 (Figs. 3, 10) shows a complete section through the aluminous alteration zone and the 20 South lens (although the alteration assemblages (3) and (4) are poorly developed to absent in this hole). The similar Zr and TiO_2 contents in the footwall and hanging wall indicate little variation in terms of host-rock composition and confirm the absence of the basaltic andesite in the hanging wall. The AI and CPI indexes show an overall increase from the footwall toward, and within (CPI), the ore zone (Fig. 10).

In the alteration box plots (Fig. 8C), the quartz-garnet-muscovite-biotite-chlorite assemblage (2) overlaps the quartz-garnet-biotite-muscovite assemblage in the upper part of the deposit (Fig. 8A) and is characterized by an increase in CPI values relative to least altered rhyolite. The samples from the quartz-staurolite-muscovite-garnet ± biotite ± pyrite (3) and quartz-muscovite-paragonite-pyrite ± kyanite (4) assemblages tend to plot toward the upper right corner of the box and resemble greenschist facies chlorite-muscovite-pyrite in less aluminous rocks (Large et al., 2001). The most intensely altered samples are dominated by the quartz-pyrite-kyanite-andalusite-chalcopyrite-gold (5) and the quartz-kyanite-andalusite-sphalerite (6) assemblages. They plot toward the upper part of the diagram, characterized by high CPI values but extremely variable AI values, as expected for the intense leaching of Na_2O, K_2O, CaO, and MgO by a very low pH fluid (Large et al. 2001) and an increase in pyrite abundance in

assemblage (5). The advanced argillic alteration index [AAAI = $100*SiO_2/(SiO_2 + 10MgO + 10CaO + 10Na_2O)$] has recently been proposed to quantify strong SiO_2 enrichment related to acid leaching (Williams and Davidson, 2004). A box plot of the AAAI versus AI (Fig. 8D) shows a well-defined trend toward the upper right corner (assemblages 1–3) and then a shift toward the upper center and left corner (assemblages 4–5). The quartz-pyrite-kyanite-andalusite-chalcopyrite-gold assemblage (5) hosts the mineralization and shows a very strong leaching with many samples showing AAAI values above 90 (Fig. 8D). The progressively lower AI values for these samples are due to strong leaching of the elements used to calculate the AI values (Williams and Davidson, 2004). The quartz-kyanite-andalusite-sphalerite assemblage (6) shows less intense acid leaching, possibly due to neutralization of the fluid by greater mixing with seawater in the upper part of the mineralized zone. Figure 13 shows isocon diagrams for each of the alteration assemblages described above. Isocon diagrams were constructed using only the assemblages derived from the rhyodacite-rhyolite in the footwall (unit 5.2b) and the average composition of the alteration facies presented in Table 5. Despite large changes in several constituents, Al_2O_3, Zr, and TiO_2 concentrations in facies 1 through 4 yield almost perfect isocons with a slope of 1:1 (Fig. 13A-D; i.e., constant volume and/or constant mass isocon). For the mineralized quartz-pyrite-kyanite-andalusite-chalcopyrite-gold (5) and the quartz-kyanite-andalusite-sphalerite (6) assemblages, Al_2O_3, and Zr define an isocon that indicates significant volume and mass gains as well as changes in the gains and losses of individual components (Fig. 13E, F). The results show a strong progressive Na_2O depletion in all assemblages (Table 1). CaO concentrations are high in the quartz-garnet- muscovite-biotite-chlorite assemblage (2) but are low in other assemblages. MnO and MgO were added in the first three alteration assemblages (Fig. 13A-C). The average Mn concentration in the garnet-rich assemblage is more than 2,100 ppm (Table 5). The abundance of sulfides, mainly pyrite, is reflected in the significant increases in $Fe_2O_{3(total)}$ and S in all assemblages. From the outer quartz-muscovite-biotite-chlorite assemblage (1) to the inner quartz-pyrite-kyanite-andalusite-chalcopyrite-gold ore zone (5), there is strong leaching of Na_2O and CaO with significant loss in K_2O and MgO in the mineralized zones (5–6). In the ore zone (5), all oxides except Al_2O_3, SiO_2, and $Fe_2O_{3(total)}$ were strongly leached, and the latter are present mainly as aluminosilicates (andalusite and kyanite) and pyrite. Similar alteration was reported by Marquis et al. (1990a, c) at Dumagami. Metamorphosed advanced argillic alteration associated with metamorphosed epithermal high-sulfidation deposits has similar geochemical characteristics (Dubé et al., 1998).

The Zn content is anomalous (–100 ppm) from the quartz-garnet-muscovite- biotite-chlorite assemblage (2) to the auriferous zone and especially within the quartz-kyanite-andalusite-sphalerite assemblage (6) above the gold-bearing zone. The gold-bearing ore zone is characterized by elevated Cu, Ag, Zn, As, and Pb in addition to Au (Tables 1, 5).

20 South lens

Mineralogy: Hydrothermal alteration assemblages in the basaltic andesite (unit 5.4) that are associated with the 20 South
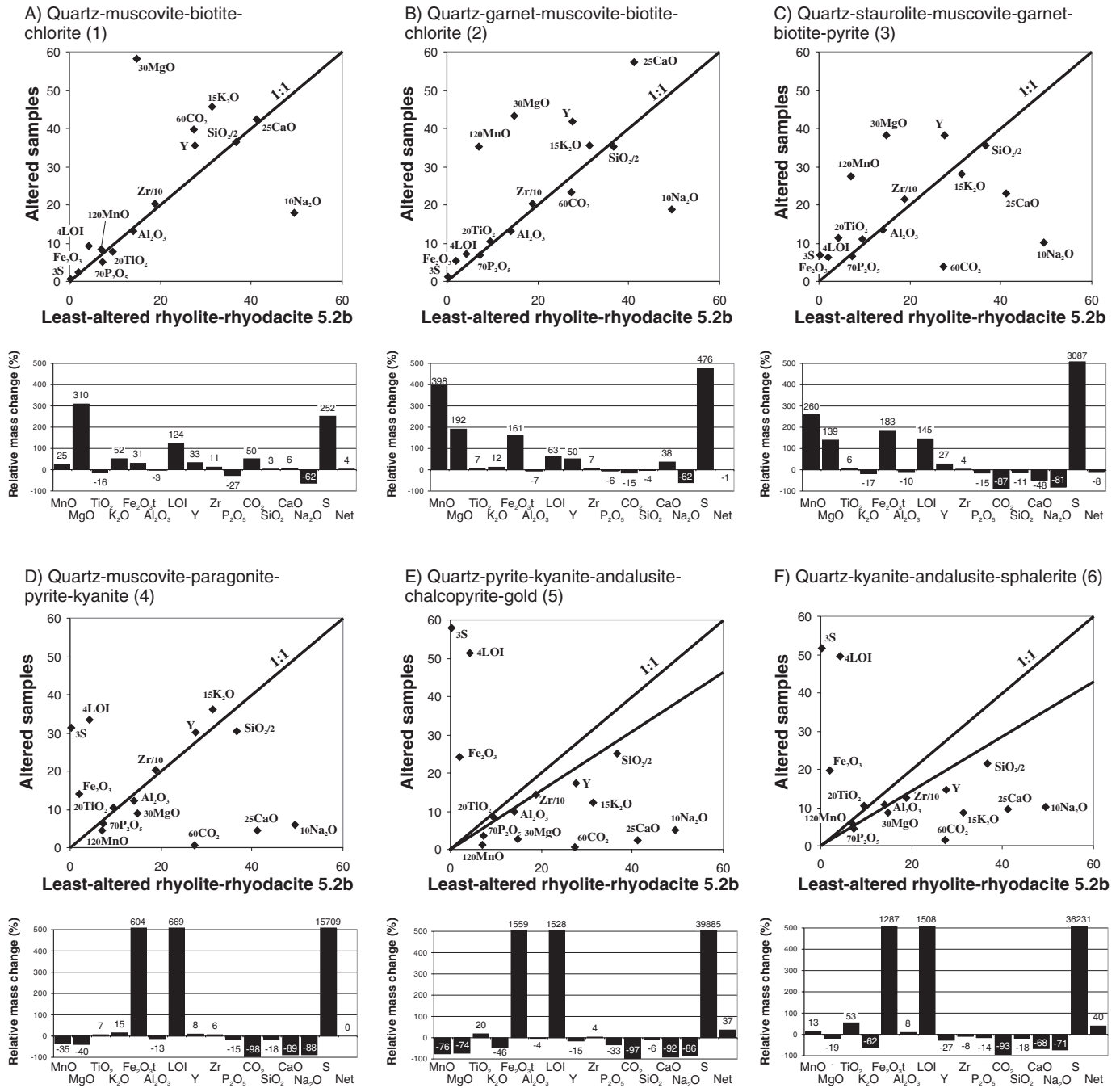
FIG. 13. Best-fit isocon diagram (Grant, 1986) with the relative mass gains and losses for the major elements quantified using equations given in Grant (1986) and the method proposed by Huston (1993) for the alteration assemblages hosted by rhyodacite-rhyolite (unit 5.2b) in the footwall of the 20N Au zone, lower levels of the deposit. Average major and minor components are plotted as wt percent of the oxides. Data for trace elements are plotted in 0.1 ppm. As suggested in Grant (1986), components are scaled for a clearer view and to show changes in components that might be considered minor relative to silica or alumina but which are useful alteration parameters. A. Quartz-muscovite-biotite-chlorite assemblage (1). B. Quartz-garnet-muscovite-biotite-chlorite assemblage (2). C. Quartz-staurolite-muscovite-garnet ± biotite ± pyrite assemblage (3). D. Quartz-muscovite-pyrite-kyanite assemblage (4). E. Quartz-pyrite-kyanite-andalusite-chalcopyrite-gold assemblage (5). F. Quartz-kyanite-andalusite-sphalerite assemblage (6).

lens are characterized by a pink quartz-biotite-rutile-titanite assemblage similar to that in the hanging wall of the 20 North lens (Fig. 12G). The alteration zone is up to a few meters wide and characterized by metasomatic and/or metamorphic layering and local hydrothermal breccia cut by numerous

pyrrhotite-pyrite-sphalerite veinlets. Toward the ore zone, the pink assemblage is gradually replaced by a proximal greenish quartz-muscovite-green mica-titanite assemblage, which hosts the sulfide minerals (Figs. 12H, 14A, B). The immediate footwall and hanging wall is a quartz-muscovite-green
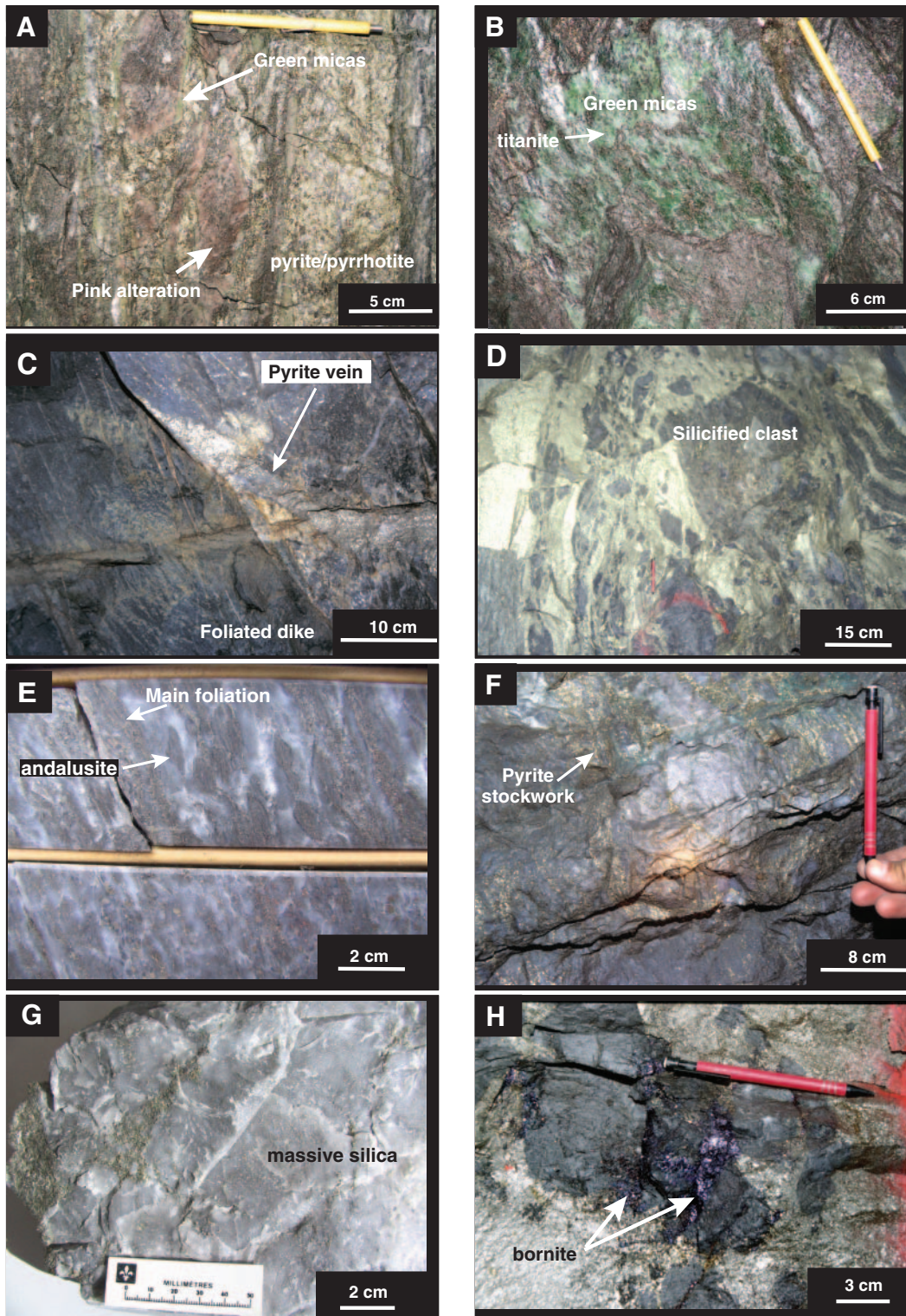
FIG. 14. A. Hydrothermal breccia, showing abundant pyrite-pyrrhotite stringers and pink quartz-biotite-rutile-titanite assemblage partially replaced by green quartz-muscovite-green mica-titanite assemblage hosting the sulfides. B. Green micas with titanite hosted by pyrrhotite-rich basaltic andesite (unit 5.4) in the hanging wall of lens 20 South (stope 106-21-80). C. Au-rich pyrite vein hosted by the Mooshla intrusion and cut by foliated postore mafic dike (section view), Doyon mine, zone West. D. Massive angular silicic clasts in massive pyrite, Bousquet 2 mine. E. Drill core sample, showing large syndeformation andalusite porphyroblasts dusted by fine pyrite in a quartz-muscovite matrix, Bousquet 2 mine. F. Massive silicic alteration cut by pyrite stockwork, Bousquet 2 mine. G. Massive silicic alteration characteristic of strong acid leaching. H. Bornite veinlets cutting a wall-rock clast within massive pyrite ore, Bousquet 2 mine.

mica-pyrite assemblage. This assemblage is 10 to 15 m wide and hosts pyrite-pyrrhotite-sphalerite veinlets (1–5 cm wide, ≤50 vol %) with variable proportions of quartz, chalcopyrite, titanite, and other minerals (Table 6). The sulfide veinlets are transposed subparallel to the main foliation. Muscovite and green mica with unoriented titanite (3 vol %, ≤3–5 mm) form millimeter- to centimeterm-wide selvages symmetrically distributed along the margins of the veinlets. The proportion of muscovite, green mica, quartz, and sulfides increases toward the ore zone The green mica is a chromium phengite with up to 0.83 percent Cr_2O_3 and 0.35 percent V_2O_3 (Table 7). Chlorite is not abundant (≤10 vol %), and biotite is absent or minor (≤5 vol %) and commonly replaced by chlorite. Less than 2 vol percent small garnet crystals associated with pyrrhotite and tourmaline are present locally.

The alteration is not as well developed in the upper felsic unit (5.5) or in the feldspar- and quartz-phyric rhyolite (unit 5.3). These rocks are characterized by a distal dark gray quartz-biotite-muscovite-garnet assemblage with up to 8 vol percent pink garnet (1–3 mm) and a proximal quartz-muscovite-pyrite ± chlorite schist with minor carbonate, epidote, biotite, and traces of garnet and tourmaline.

Lithogeochemistry: Geochemical analyses of the alteration assemblages associated with the 20 South lens compared to the least altered host rock are given in Table 8. The quartz-biotite-rutile-titanite assemblage is characterized by high contents of $Fe_2O_{3(total)}$, S, Zn, and B, and a slight increase in K_2O compared to least altered rocks (Table 8). It is very similar to the pink alteration developed in the hanging wall of the 20 North lens. Na_2O averages 4.84 wt percent (3.5–6 wt %) compared to 5.15 wt percent for the least altered basaltic andesite. The quartz-muscovite-green mica-titanite assemblage shows a relative increase in K_2O, S, and $Fe_2O_{3(total)}$, and a small decrease in Na_2O, MgO, and CaO. However, in comparaison to the other alteration types, the geochemical variations are limited. Al_2O_3, TiO_2, Zr, and Y were the least mobile elements in both the quartz-biotite-rutile-titanite and the quartz-muscovite-green mica-titanite assemblages and define a best-fit isocon that indicates a slight mass gain and/or volume gain (Fig. 15A-B). $Fe_2O_{3(total)}$, CO_2, K_2O, and S were added in both assemblages with losses of MgO and some minor losses of CaO and SiO_2 in the quartz-muscovite-green mica-titanite assemblage (Fig. 15A, B, Table 6). There has been some

increase in Zn, whereas Sn, Sb, and Bi were leached (Table 8). Figure 15A combined with Table 8 indicate that overall there is no gain in Na_2O in the pink quartz-biotite-rutile-titanite assemblage.

TABLE 7. Microprobe Analyses of Green Micas (Cr phengite)

Oxide (%)	093-1-M1	093-1-M2	093-1-M3	093-3-M1	093-3-M2	093-3-M3
SiO_2	45.25	45.06	44.76	44.55	45.43	45.27
Al_2O_3	31.94	31.65	32.23	32.19	32.75	31.83
FeO	2.50	2.30	2.45	2.47	2.11	2.31
MgO	1.25	1.30	1.24	1.20	1.10	1.36
MnO	0.01	<0.01	0.11	<0.01	0.04	0.01
Cr_2O_3	0.82	0.63	0.52	0.59	0.30	0.83
TiO_2	0.67	0.67	0.55	0.55	0.60	0.60
V_2O_3	0.31	0.20	0.35	0.09	0.23	0.20
K_2O	9.93	9.93	9.89	9.88	10.16	9.67
Na_2O	0.60	0.66	0.71	0.78	0.48	0.74
CaO	0.01	<0.01	<0.01	<0.01	<0.01	<0.01
BaO	0.52	0.54	0.02	<0.01	<0.01	0.41
F	0.31	0.35	0.27	0.31	0.23	0.43
Cl	<0.01	0.02	<0.01	<0.01	<0.01	0.03
Total	94.12	93.31	93.10	92.61	93.43	93.69
TOT-O	93.99	93.16	92.99	92.48	93.33	93.50

Number of ions on the basis of 24 (O, OH)

Si	6.206	6.231	6.180	6.182	6.221	6.226
Al	1.794	1.769	1.820	1.818	1.779	1.774
Total	8.000	8.000	8.000	8.000	8.000	8.000
Al	3.368	3.388	3.425	3.447	3.507	3.386
Fe^{2+}	0.287	0.266	0.283	0.286	0.241	0.265
Mg	0.255	0.269	0.255	0.248	0.224	0.279
Mn	0.002	0.000	0.013	0.000	0.004	0.001
Cr	0.089	0.069	0.056	0.065	0.032	0.090
Ti	0.069	0.069	0.057	0.057	0.061	0.062
V	0.034	0.022	0.038	0.010	0.025	0.022
Total	4.104	4.083	4.127	4.113	4.094	4.105
K	1.737	1.751	1.742	1.749	1.775	1.696
Na	0.160	0.177	0.189	0.211	0.129	0.198
Ca	0.002	0.000	0.000	0.000	0.001	0.000
Ba	0.028	0.029	0.001	0.000	0.000	0.022
Total	1.927	1.957	1.932	1.960	1.905	1.916
F	0.136	0.152	0.120	0.134	0.100	0.186
Cl	0.000	0.004	0.001	0.000	0.000	0.008
Total	0.136	0.156	0.121	0.134	0.100	0.194

TABLE 6. Summary of the Mineralogy and Mass Gains and Losses Within the Various Metamorphosed Hydrothermal Alteration Assemblages at LaRonde Penna[1]

Main mineralogical assemblage	Associated minerals	Main chemical changes
20 South lens: Upper and intermediate levels		
Footwall and hanging wall (hosted in 5.4 andesite)		
Quartz-biotite-rutile/titanite	Tourmaline, calcite, garnet, epidote, hornblende, chloritoid, muscovite	Losses: Very minor MgO; Sn, Bi Gains: S, CO_2, $Fe_2O_{3(total)}$, K_2O, Zn, Au, B
Quartz-muscovite-green micas-pyrite	Titanite pyrite, chalcopyrite, tourmaline feldspar, margarite, clinozoïsite, Mg chlorite, carbonates	Losses: MgO, Na_2O, ±MnO, CaO, SiO_2, Sn, Bi Gains: S, CO_2, $Fe_2O_{3(total)}$ K_2O, Au, Zn

[1] Based on Table 8 and Figure 15

TABLE 8. Average Composition of Alteration Facies in Footwall and Hanging Wall of the 20 South Lens, Upper and Intermediate Levels of the LaRonde Penna Mine

| Facies | Footwall and hanging wall of 20 south (hosted in 5.4 andesite) | | | | | | | | | Footwall and hanging wall of 20 south (hosted in 5.5b rhyolite) | | | | | | | | |
| | basaltic andesite least altered 5.4 | | | qtz-bio-rut-tit | | | qtz+mus+gm+tit | | | upper felsic unit least altered 5.5 | | | qtz-bio-mus-grt | | | qtz-mus-py | | |
(%)	Average	STD	No.	Average	STD	No.	Average	STD	No.	Average	STD	No.	Average	STD	No.	Average	STD	No.
SiO_2	56.83	4.08	8	51.30	9.84	8	51.54	9.96	17	70.43	1.54	5	67.14	3.45	5	64.83	15.04	3
TiO_2	1.11	0.12	8	0.99	0.13	8	1.06	0.24	17	0.37	0.13	5	0.71	0.11	5	0.44	0.23	3
Al_2O_3	20.36	1.23	8	18.11	2.70	8	19.36	3.68	17	14.39	0.50	5	14.76	0.66	5	13.40	1.06	3
$Fe_2O_{3(total)}$	4.68	2.43	8	11.36	7.42	8	9.89	11.32	17	2.52	0.34	5	4.99	2.79	5	8.56	10.73	3
MnO	0.07	0.03	8	0.06	0.03	8	0.06	0.03	17	0.06	0.02	5	0.37	0.53	5	0.03	0.02	3
MgO	3.14	1.24	8	2.68	1.26	8	2.03	1.05	17	0.94	0.52	5	1.40	0.64	5	0.64	0.09	3
CaO	5.10	2.17	8	4.45	2.30	8	4.57	3.74	17	3.08	0.97	5	3.41	0.66	5	1.12	1.24	3
Na_2O	5.15	1.16	8	4.84	1.16	8	4.17	1.54	17	1.95	1.12	5	1.93	0.62	5	1.31	0.62	3
K_2O	1.12	0.64	8	1.36	1.04	8	2.00	1.37	17	3.13	0.33	5	2.20	0.85	5	2.72	0.88	3
P_2O_5	0.12	0.02	8	0.11	0.04	8	0.11	0.07	17	0.09	0.07	5	0.14	0.01	5	0.08	0.04	3
LOI	1.84	0.65	8	3.92	2.24	8	4.92	3.61	17	1.57	0.52	5	1.57	0.42	5	5.55	5.74	3
Total (%)	99.72	0.65	8	99.36	1.27	8	99.92	1.15	17	99.32	0.59	5	99.04	0.43	5	99.09	1.64	3
S (%)	0.80	0.70	8	4.86	3.69	8	4.98	6.87	17	0.27	0.22	5	0.40	0.55	5	6.27	8.84	3
CO_2 (%)	0.16	0.28	8	0.48	1.02	8	1.04	2.82	17	0.36	0.30	5	0.20	0.12	5	0.04	0.05	3
AI	29.46	6.83	8	29.58	10.76	8	34.70	15.79	17	44.68	4.49	5	40.45	4.87	5	60.50	23.77	3
CCPI	53.20	10.60	8	61.48	23.95	8	56.63	19.46	17	40.78	7.95	5	58.32	16.28	5	55.65	25.89	3
Metals (ppm)																		
Au (ppb)	5	7	8	39	69	8	28	37	17	3	2	5	12	20	5	103	129	3
Cu	93	24	8	127	67	8	110	83	17	11	5	5	8	3	5	87	105	3
Ag	1	1	8	1	1	8	1	1	17	b.d.	b.d.	5	2	3	5	2	1	3
Zn	62	31	8	181	136	8	250	531	17	66	60	5	96	62	5	114	83	3
Pb	23	54	8	19	24	8	30	88	17	5	6	5	6	10	5	93	99	3
As	9	3	6	13	9	5	14	12	9	10	b.d.	5	10	b.d.	5	24	24	3
Sb	2	2	6	1	b.d.	5	1	b.d.	9	2	3	5	b.d.	b.d.	5	1	b.d.	3
Sn	109	287	8	8	3	6	8	3	14	155	330	5	5	b.d.	5	5	b.d.	3
Trace elements (ppm)																		
V	305	22	7	253	55	8	271	48	17	24	10	5	21	10	5	40	25	3
Ba	282	98	7	264	221	8	380	229	17	739	147	5	539	197	5	359	75	3
Cr	91	21	8	112	37	8	120	58	17	5	5	5	3	2	5	4	3	3
Mn	454	214	7	429	249	6	394	231	14	410	138	5	2683	3868	5	202	116	3
B	137	82	6	214	246	5	79	70	9	184	280	5	26	12	5	45	42	3
Bi	44	115	8	4	1	6	4	2	14	10	15	5	3	b.d.	5	6	6	3
Y	12	3	8	10	3	8	10	8	17	20	2	5	38	10	5	24	10	3
Zr	51	20	8	47	15	8	62	39	17	169	16	5	201	27	5	171	58	3

Notes: SiO_2, TiO_2, Al_2O_3, $Fe_2O_3^T$, MnO, MgO, CaO, Na_2O, K_2O, P_2O_5, LOI, Y, Zr = ICP-AES (INRS), Ag, Cu, Zn, Pb, Sn, V, Ba, Cr, Mn, Bi = ICP-80 (XRAL), Au (ppb) = Fire Assay (XRAL), As, Sb = Fusion/ICP/Hybride AA (XRAL), S = Leco (XRAL), CO2 = Coulometry (XRAL), B = ICP90A (XRAL), bio = biotite, cpy = chalcopyrite, chl = chlorite, gm = green micas, grt = grenat, mus = muscovite, qtz = quartz, rut = rutile, sta = staurolite, tit = titanite, STD = standard deviation, No. = number of analyses, AI: Alteration Index (Ishikawa et al., 1976); CCPI: chlorite-carbonate-pyrite alteration index (Large et al., 2001), b.d. = below detection
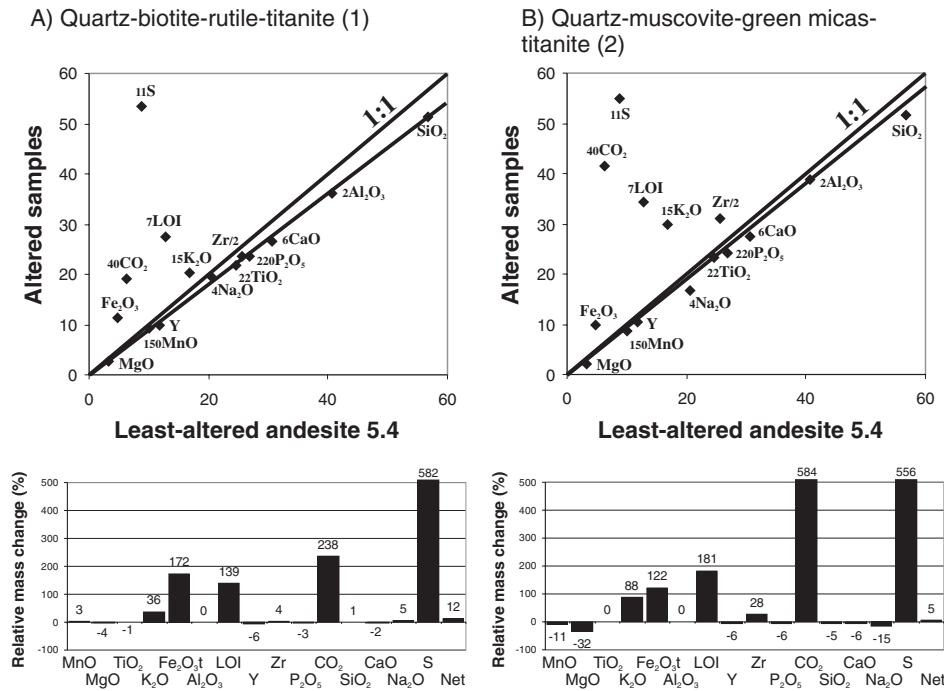
FIG. 15. Best-fit isocon diagram (Grant, 1986) with the relative mass gains and losses for the major elements quantified using equations given in Grant (1986) and the method proposed by Huston (1993) for alteration assemblages hosted by basaltic andesite (unit 5.4) in the footwall and hanging wall of lens 20 South, intermediate to upper levels of the deposit. Major and minor components are plotted as wt percent of the oxides. Data for trace elements are plotted in 0.1 ppm. As suggested in Grant (1986), components are scaled for a clearer view and to show changes in components that might be considered minor relative to silica or alumina but which area useful alteration parameters. A. Quartz-biotite-rutile-titanite assemblage. B. Quartz-muscovite-green mica-titanite assemblage.

In the upper felsic unit (5.5), the quartz-biotite-muscovite-garnet assemblage is enriched in MnO (2,680 ppm), $Fe_2O_{3(total)}$, and S and has lost some K_2O, B, and Ba. The quartz-muscovite-pyrite ± chlorite assemblage adjacent to the ore is characterized by low CaO, Na_2O, and MgO, elevated $Fe_2O_{3(total)}$, and S and anomalously high Au, Cu, Zn, and Pb values (Table 8).

Zones 7 and 6

The footwall alteration associated with zone 7 is characterized by a banded quartz-plagioclase-biotite-hornblende assemblage with ≤5 to 8 vol percent pink garnet (1–10 mm). Garnet abundance increases to the south toward the mineralized zones. The latter corresponds to a bleached quartz-muscovite-chlorite-pyrite schist with local traces of garnet and green mica (when hosted by unit 5.1b(b) andesite sills). This alteration contains ≤10 to 20 vol percent pyrite-sphalerite ± chalcopyrite veinlets (≤1 cm) transposed parallel to the main foliation. It is generally anomalous in gold (≤1 g/t Au), with up to 10 to 20 g/t Ag and trace amounts to 1 wt percent Cu and/or Zn. On level 170 (1,700-m depth), zone 7 forms a massive sulfide lens essentially composed of pyrite with some chalcopyrite and sphalerite (Figs. 3, 4F). It is auriferous, with parts running up to 19 g/t Au, 69 g/t Ag, 0.69 percent Cu, and 2.74 percent Zn over 4.5 m. The hanging wall of this lens consists of a quartz-muscovite-garnet schist transitioning upward to altered pink unit 5.1b andesite. This pink alteration is similar to the assemblage in the hanging wall of the 20N Zn zone.

As in the 20 North and 20 South lenses, the alteration associated with zone 7 gradually changes with depth in the mine, becoming more aluminous, with quartz, staurolite, biotite, and garnet in the footwall. The ore zone is hosted by a quartz-muscovite-staurolite-andalusite-biotite-garnet schist.

The footwall of zone 6 consists of a distal quartz-garnet-chlorite assemblage and a proximal quartz-muscovite schist with disseminated pyrite. The mineralized zone is hosted by a quartz-muscovite-pyrite ± chlorite schist with transposed pyrite ± sphalerite ± chalcopyrite veinlets and local meter-thick auriferous pyrite-sphalerite ± chalcopyrite massive sulfide lenses (e.g., 6.28 g/t Au, 0.18 wt % Cu and 4.4 wt % Zn over 2.8 m in DDH 3146-02). The immediate hanging wall is a quartz-muscovite schist, whereas a pink quartz-muscovite-biotite-rutile-titanite assemblage is located farther away from the mineralized zones. Similar to the other ore zones, at greater depth in the mine, zone 6 becomes more aluminous with the presence of staurolite andalusite, pyrophyllite, and kyanite.

Discussion

As proposed elsewhere in the district (e.g., Tourigny et al., 1989; Stone, 1990; Marquis et al., 1990a), the alteration assemblages in the LaRonde Penna mine area are interpreted to be synvolcanic. Their distribution relative to the orebody indicates that they are metamorphic products of original synvolcanic hydrothermal alteration associated with a VMS hydrothermal system. The alteration minerals have been

recrystallized to upper greenschist-lower amphibolite grade by syn- to late, main-stage deformation and metamorphism. At LaRonde Penna, the preferred elongation of metamorphic minerals such as garnet, andalusite, kyanite, and staurolite and the orientation of the gangue inclusions parallel to the main foliation indicate that these minerals are syn- to late, main-stage deformation.

The quartz-garnet-biotite-muscovite assemblage of the footwall is thought to be the metamorphosed equivalent of the magnesium-rich sericite-chlorite alteration zone typical of Noranda-type VMS deposits, which have experienced only lower greenschist facies metamorphism (Morton and Franklin, 1987). Although the quartz-muscovite assemblage is likely a metamorphosed equivalent of quartz-sericite alteration at Noranda (cf. Barrett and MacLean, 1994) the abundance of aluminosilicates at depth in the mine indicates that LaRonde Penna is not a typical Noranda-type VMS deposit. Unlike other polymetallic Au-rich VMS deposits (Hannington et al., 1999; Huston, 2000), hydrothermal feldspar-bearing assemblages are not present. Only traces of hydrothermal plagioclase in transposed sulfide-rich stringers in the footwall and hanging wall of the 20 North lens were identified.

At LaRonde Penna, the garnets have not grown from primary sedimentary or diagenetic nodular accumulations of Mn oxide minerals, as originally proposed by Valliant and Barnett (1982). Rather, the Mn-rich garnet zone in the footwall of the 20 North lens is thought to reflect alteration formed by higher temperature fluids. Irrespective of the formation process, the Mn-rich garnet zone is a good visual guide to the 20 North Au zone. We speculate that the Mn enrichment of the garnets results from the replacement and leaching of manganiferous Fe carbonate, which is locally present as disseminations below the 20 North lens, in particular within the unit 3.0 scoriaceous tuff of the lower member of the Bousquet Formation (Lafrance et al., 2003). During ascent, the fluid may have leached the Mn from the carbonates and deposited it in secondary clays or phyllosilicates (e.g., chlorite) associated with synvolcanic hydrothermal alteration closer to the main ore zone; later metamorphism may then have concentrated the Mn within the garnet and the chloritoid. Stone et al. (1988) proposed that the Mn-rich garnet in the district is a product of recrystallization of manganiferous ilmenite to spessartite-almandine and rutile, but no evidence of such recrystallization was found at LaRonde Penna. The most likely source of the garnet is a Mn-rich chlorite alteration zone.

In terms of major elements, the two most prominent geochemical features of the hydrothermal system in the intermediate to upper parts of the mine are the Na_2O leaching typically associated with proximal alteration in VMS deposits (cf. Franklin et al., 1981; Franklin, 1996; Large et al., 2001) combined with the increase in MnO in the footwall of the 20 North lens. At depth in the mine, the increase in MnO combined with the strong to complete Na_2O, CaO, MgO, and K_2O leaching constitute the best geochemical footprints of the hydrothermal system. In the intermediate and upper parts of the mine, Mn garnet and biotite are the most conspicuous alteration minerals in the footwall, whereas in the lower part of the orebody, Mn-garnet, zincian staurolite, kyanite, and andalusite with coarse pyrite are the dominant minerals. The zincian staurolite is similar to that present in certain other base metal-enriched hydrothermal systems (e.g., Huston and Paterson, 1995).

Comparison of LaRonde Penna with other VMS deposits

Although the LaRonde Penna deposit is distinct from many other VMS deposits, the geologic setting of the deposit is similar to the bimodal, felsic-dominated class of VMS deposits proposed by Barrie and Hannington (1999). The stratigraphic succession at LaRonde Penna contains more than 50 percent transitional to calc-alkaline felsic volcanic and volcaniclastic rocks with less than 20 percent mafic strata (Lafrance et al., 2003; Mercier-Langevin et al., 2004). The extensive footwall alteration, characterized by Na leaching and Mn enrichment, and the predominantly Zn-rich metallic signature with significant Ag, Pb, and Au are all consistent with the bimodal-felsic group. However, the size of the deposit and the Au grade are significantly greater than the average Archean bimodal-felsic deposits (7.1 Mt at 6.23% Zn and 0.83 g/t Au: Barrie and Hannington, 1999). The presence of the aluminous alteration hosting the 20 North gold mineralization at depth in the mine is also atypical of the bimodal-felsic group.

The LaRonde Penna deposit has some similarities to the Zn-Pb-Cu–rich Mattabi-type VMS deposits of the Superior province (Morton and Franklin, 1987); in particular, the presence of a high proportion of felsic fragmental volcanic rocks in the footwall and the abundance of andalusite, kyanite, and chloritoid are similar. However, the absence of iron-carbonate and the high concentration of gold at LaRonde Penna differs significantly from typical Mattabi-type VMS deposits.

In terms of metal association, most Au-rich volcanic-hosted massive sulfide deposits fit into three groups: (1) a Au-Zn-Pb-Ag association in which Au is concentrated toward the top or along the margins of the massive sulfide lens, (2) a Au-Cu association where Au is concentrated at the base of the massive sulfide lens or within the underlying stringer zone, and (3) a pyritic Au group where Au is concentrated within massive pyrite zones with low base metals content (Huston and Large, 1989; Poulsen and Hannington, 1995; Hannington et al., 1999). At LaRonde Penna, both the Au-Cu association (zone 20 North Au) and the Au-Zn-Pb-Ag association (20 South lens) are represented. In contrast to the 20 North lens, gold in the 20 South lens is concentrated within the Zn-rich massive sulfides and thus is similar to the Rosebery deposit in Australia (cf. Huston and Large, 1988). The variation from pyrite-sphalerite-pyrrhotite-chalcopyrite (Zn-Au-Cu) massive sulfide lenses with garnet-biotite alteration to a quartz-kyanite-andalusite-chalcopyrite (Au-Cu) replacement-stockwork zone at depth in the mine is interpreted to indicate variable contributions of seawater- (neutral) versus magmatic-dominated (acidic) fluids, respectively, both of which appear to have carried gold.

The metamorphosed alteration assemblages at LaRonde Penna have some features in common with the assemblages in the footwall of the metamorphosed Snow Lake VMS deposits (e.g., Chisel Lake deposit Zn-Au-Cu-Ag, 7.2 Mt at 1.7 g/t Au), which are characterized by similar biotite-garnet, chlorite-staurolite, and muscovite-kyanite zones (Galley et al., 1993). The garnet (almandine) at Snow Lake contains significant Mn and Ca, as at LaRonde Penna. The hanging-wall alteration of the Chisel Lake deposit, quartz-biotite-pyrrhotite

with amphibole and garnet, has some similarity to the quartz-rutile-titanite-biotite-chlorite assemblage with pyrrhotite-pyrite stringers in the hanging wall of the 20 North lens.

The lower part of the LaRonde Penna deposit is also similar, in terms of geologic setting and nature of the alteration, to the Paleoproterozoic Boliden deposit, a controversial Au-rich deposit, variably interpreted as a replacement metamorphic deposit (Ödman, 1941), a synvolcanic exhalative deposit (Rickard, 1986), a subsea-floor replacement deposit (Allen et al., 1996), a high-sulfidation epithermal deposit (Bergman Weihed et al., 1996), and a subsea-floor replacement deposit transitional between a VMS and a high-sulfidation deposit (Doyle and Allen, 2003). As at LaRonde Penna, Boliden is hosted by andalusite-sericite-quartz assemblages derived from dacite-rhyodacite calc-alkaline volcanic rocks near the interface with a sedimentary sequence (Ödman, 1941; Nilsson, 1968; Bergman Weihed et al., 1996; Hallberg, 2001). However, the abundance of arsenopyrite within the predeformation massive pyrite ± arsenopyrite ore at Boliden is unique.

The plagioclase-quartz-rutile and/or anatase-titanite-biotite ± chlorite alteration in the hanging wall of the 20 North lens and in the footwall and hanging wall of 20 South lens may be analogous to the quartz-albite ± chlorite alteration in the hanging wall of the Henty Au-rich massive sulfide deposit (Callaghan, 2001). The composition of green micas in the footwall and hanging wall of the 20 South lens is very similar to that of the green mica present at Que River and in the hanging wall at Hellyer (Gemmell and Fulton, 2001). The limited geochemical variations in the host rocks of the 20 South lens at LaRonde Penna are similar to those in the hanging wall fuchsite-carbonate alteration hosted by basalt at the Hellyer VMS deposit (Gemmell and Fulton, 2001). The proximal depletion of Na and K and the gain in Zn, Ca, and Mn peripheral to the aluminous ore zone at depth are similar to geochemical variations found at the high-sulfidation Cu-Au Western Tharsis deposit in the Mt Lyell field, Tasmania (Huston, 2000; Huston and Kamprad, 2000). The overall results of the lithogeochemical study of the aluminous alteration at LaRonde Penna are also very similar to those presented by Williams and Davidson (2004) for the Basin Lake prospect, also in western Tasmania.

Aluminous alteration

The aluminous alteration at LaRonde Penna is interpreted to be the metamorphic equivalent of an advanced argillic alteration assemblage common to metamorphosed high-sulfidation deposits. Such alteration is produced by corrosive leaching by acidic, relatively oxidized, and sometimes sulfur-rich fluids that may be of magmatic origin or the product of shallow boiling (Hedenquist and Lowenstern, 1994; Sillitoe et al., 1996). The aluminous alteration at LaRonde Penna is similar to that of a class of Au-rich VMS characterized by aluminous alteration (Sillitoe et al., 1996). It is also similar to the andalusite-kyanite-pyrophyllite alteration developed in the footwall and hanging wall of the Bousquet 1 deposit (Valliant et al., 1983; Tourigny et al., 1989) and in the footwall of the Bousquet 2-Dumagami deposit (Marquis et al., 1990a, c). In these deposits, the aluminosilicate-bearing rocks envelope the ore zones. At the Dumagami mine the aluminous alteration zones and the gold-poor massive sulfides also have been

interpreted as the product of interaction of felsic volcanic rocks with an acid hydrothermal fluid.

Retrograde alteration of andalusite to kyanite and/or pyrophyllite at LaRonde Penna has been documented at the district scale in several deposits (Valliant et al., 1983; Stone et al., 1988; Marquis et al., 1990a; Tourigny et al., 1993). This retrograde alteration is most likely associated with isobaric cooling due to the decrease in temperature during the waning stage of postpeak tectonometamorphism.

Timing of gold introduction

Several key observations suggest that the gold deposition was contemporaneous with the deposition of the base metals during the formation of the VMS at LaRonde Penna.

1. Despite extensive metamorphic recrystallization and deformation, a crude metal zoning of Cu, Zn, Pb, Ag, and Au, which mimics primary metal zonation in less deformed massive sulfides, is still evident in the massive sulfide lenses, together with an intimate association of Au with base metals (Figs. 7, 10; Dubé et al., 2004; Mercier-Langevin, 2005).
2. The presence of Au-bearing sulfide-rich clasts (containing up to 6 g/t Au) in a debris flow stratigraphically above a massive sulfide lens (zone 6) mined at LaRonde shaft 2 is also key evidence of predeformation Au-rich VMS mineralization (Mercier-Langevin, 2005; Fig. 16). At the Dumagami mine, the gold was thought to have been introduced after deposition of massive sulfides, during later brittle deformation and associated retrograde metamorphism and alteration (Marquis et al., 1990a). One of the main arguments for the late-stage introduction of gold was the lack of direct evidence that the aluminous alteration was gold-bearing (Marquis et al., 1990a). At LaRonde Penna, the aluminous alteration coincides directly with quartz-pyrite-kyanite-andalusite-chalcopyrite-gold ore (Table 5). Thus, the Au-base metal association and field relationships strongly suggest the formation of a polymetallic Au-rich VMS system (Dubé et al., 2003, 2004; Mercier-Langevin et al., 2007a). Synvolcanic Au and base metals also have been locally remobilized and concentrated during superimposed deformation-metamorphism events (Dubé et al. 2004), similar to what has been proposed by Tourigny et al. (1993) and Teasdale et al. (1996) in the nearby Bousquet 2-Dumagami deposit. However, late-stage introduction of gold has not been recognized.

Proposed formation model

The detailed geologic reconstruction of the volcanic sequence of the LaRonde Penna ore lenses (Mercier-Langevin et al., 2007a) strongly suggests that the formation and size of the large 20 North lens is related, at least in part, to the presence of the basaltic andesite (gabbroic sill-dike complex, unit 5.4) and the feldspar- and quartz-phyric rhyolite (unit 5.3) in its hanging wall (Fig. 3). The massive basaltic andesite and the cooling rhyolite are thought to have insulated the hydrothermal cell from rapid advective cooling. This allowed retention of the mineralized hydrothermal fluid over a longer period of time and also promoted subsea-floor deposition of sulfide minerals by largely restricting upward fluid flow to unit 5.2b. This resulted in subsea-floor replacement (Doyle and Allen, 2003) of the underlying unit 5.2b rhyodacitic to
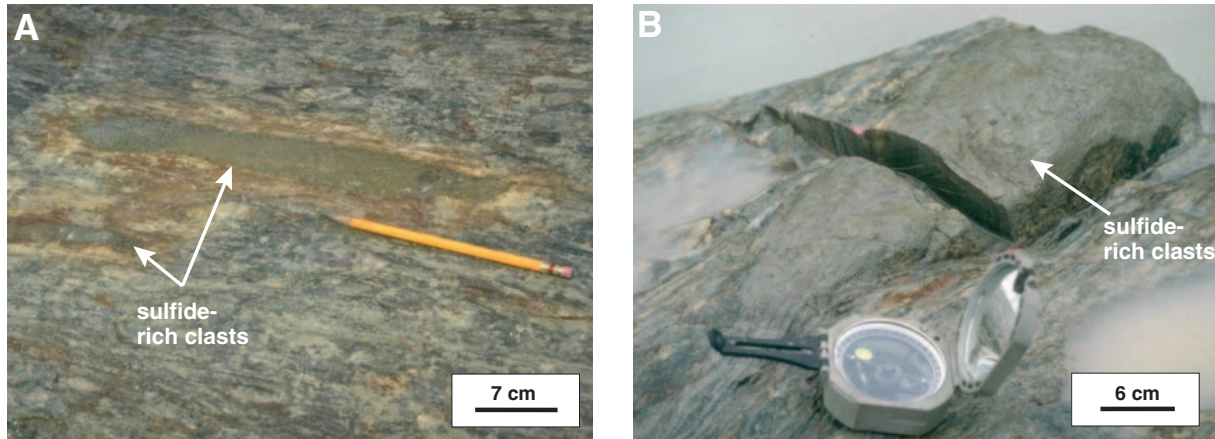
Fig. 16. A. Outcrop photograph of sulfide-rich clasts within a debris flow stratigraphically above the massive sulfides lens of zone 6 mined at the LaRonde 2 shaft. B. Close up of a sulfide-rich clast. Photographs from Agnico-Eagle Mines Ltd.

rhyolitic breccias, the latter acting as a permeable horizon within the volcanic complex in which the sulfides were deposited by infiltration, precipitation, and replacement of the host rocks.

The distribution of the 20 North, 20 South, 6 and 7 mineralized zones, and their alteration assemblages suggests a stacking of sulfide lenses within a single hydrothermal upflow zone within the upper portion of the Bousquet Formation (Fig. 3). Figure 17A is a schematic illustration of the interpreted predeformation geologic-hydrothermal setting and distribution of the sulfide lenses and the superposition of the associated metamorphosed alteration assemblages in the intermediate to upper part of the LaRonde Penna deposit. Figure 17B depicts the prominent hanging-wall alteration and pyrrhotite-pyrite network of veinlets which indicate that the hydrothermal system hydraulically fractured and permeated into the hanging-wall units, forming a hydrothermal alteration "plume" that extends from the stratigraphic hanging wall of the 20 North lens upward to the footwall of 20 South. This stockwork zone defines the fluid-flow path through higher stratigraphical levels.

In the proposed long-lived hydrothermal model, zones 6 and 7 formed in the lower part of the upper member of the Bousquet Formation. Focused fluid flow continued through these zones to higher stratigraphic levels until the fluids reached the sea floor. Subsea-floor deposition of sulfides in the more permeable rhyodacite-rhyolite flow-breccia deposits (unit 5.2b) was contemporaneous with the deposition of lenses of graphitic argillite as illustrated by their presence in the upper part of the 20 North lens. This stage of sulfide emplacement was aided by the emplacement of the less permeable feldspar and quartz-phyric rhyolite (unit 5.3) and basaltic-andesite (unit 5.4) on top of the 20 North lens. We speculate that this cap likely sealed the hydrothermal system and created a ponding effect within the underlying 5.2b rhyodacite-rhyolite. This forced the hydrothermal fluids to evolve thermally and chemically, enhancing ore mineral growth and zone refining (e.g. Ohmoto, 1996) and contributing to the formation and size of the large 20 North lens. Building of fluid pressure and overpressuring of the lithologic cap promoted upward fluid migration to form the 20 South

lens closer to the sea floor, as demonstrated by the pyrrhotite-pyrite stringers and pinkish alteration assemblages from the top of the 20N Zn zone to the base of the 20 South lens. This model is consistent with the syngenetic subsea-floor replacement model of Doyle and Allen (2003), and implies continuous hydrothermal activity during construction of the volcanic pile with possible sequential near-sea-floor deposition. The
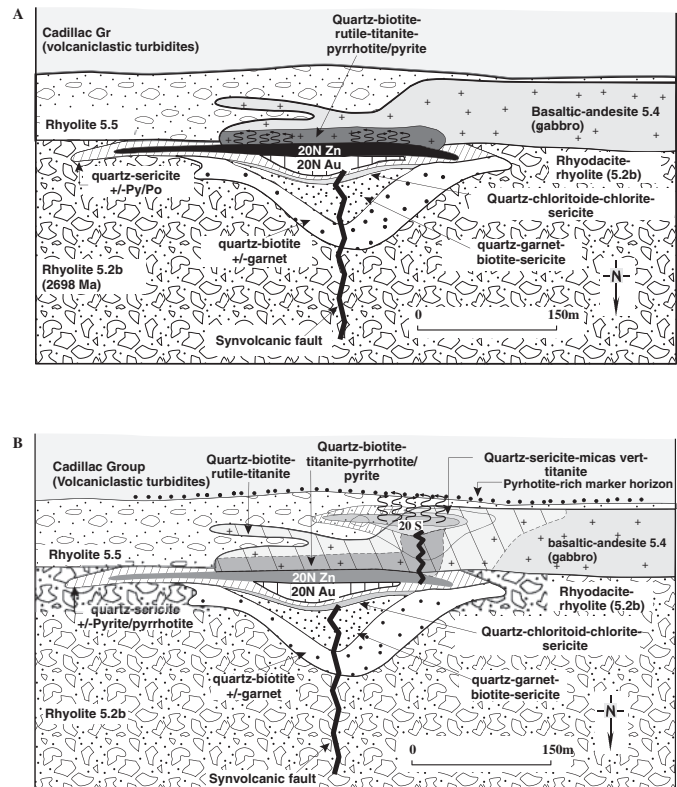

Fig. 17. Schematic east-west section, showing the possible predeformation architecture of the LaRonde Penna deposit at 1,460 m below surface (intermediate level), showing the position of the different mineralized lenses, the stratigraphy, and the postdeformation alteration assemblages. A. Formation of the 20 North lens. B. Formation of the 20 South lens. 20N Zn = 20 North Zn zone, 20N Au = 20 North Au zone, 20 S = 20 South lens.

well developed aluminous alteration in both the footwall and hanging wall of the ore zone at depth also is compatible with a subsea-floor replacement model.

The advanced argillic alteration represents the lateral westward extension of the 20 North lens present in the upper and intermediate levels of the mine. This is supported by the recent discovery of Au-Zn–rich massive sulfide zones within the advanced argillic alteration zone at depth (14 m at 5.7 g/t Au and 6.4 wt % Zn in drill hole 3215-99: Agnico-Eagle Mines Ltd. Press release February 23, 2005). We speculate that the change in the alteration and mineralization styles at depth in the mine is associated with the presence of a rhyolite dome/cryptodome in the footwall of the lens (unit 5.2; Mercier-Langevin et al., 2007a), which likely provided heat and fluids to the hydrothermal system in this specific area. Thus, the proximity of a magmatic chamber (subvolcanic intrusion), a rhyolite dome and/or cryptodome, and synvolcanic faults where acid fluids of a possible magmatic origin were focused and not completely neutralized by seawater, contributed to the intense aluminous alteration and the enrichment of gold in the volcanic edifice.

At the district scale, the role of the multistage synvolcanic Mooshla intrusive event in providing metals and/or heat to initiate or maintain the hydrothermal fluid circulation may also have been critical (Valliant and Hutchinson, 1982). The pre-main–stage deformation auriferous quartz-sulfide–rich veins at the Doyon mine, hosted in part by the Mooshla intrusive complex (Fig. 14C), are potentially genetically related to this synvolcanic intrusion (Gosselin, 1998; Galley et al., 2003). In such a model, the auriferous quartz-sulfide–rich veins at the Doyon mine could represent the end-member magmatic volatile-induced mineralization (intrusion related) in proximity to the source intrusion. The synvolcanic Mooshla intrusive complex is located in the core of the Bousquet Formation (Lafrance et al., 2003) and may have been the main eruptive center and may also have been involved in the district-scale hydrothermal system. The magmatic event represented by the emplacement of the Mooshla intrusion may have had an equivalent in the LaRonde area that has been dislocated by ensuing tectonism in the footwall of the deposit (Fig. 1B). This subvolcanic intrusive event is represented by the concentration of felsic dome complexes in the LaRonde area.

The LaRonde-Bousquet 2 Au-rich VMS complex

The LaRonde Penna and Bousquet 2-Dumagami deposits are interpreted to have been related to the same large hydrothermal system. The Bousquet 2-Dumagami deposit (Marquis et al., 1990a-c; Tourigny et al., 1993; Teasdale et al., 1996) is composed of massive and semimassive pyrite lenses, with Au-Ag-Cu-Zn mineralization, in the core of a semiconformable aluminous alteration zone (Fig. 14D). This alteration grades outward into a distal quartz-biotite-muscovite-garnet-carbonate-chlorite and/or chloritoid assemblage, which is gradually overprinted by a quartz-muscovite ± garnet assemblage. The ore zone is associated with a proximal quartz-andalusite-muscovite-pyrite assemblage (Fig. 14E) and a discrete (tens of meters wide) massive silicic replacement breccia zone containing up to 97 wt percent SiO_2 and transposed pyrite stringers (Fig. 14F, G; Tourigny et al., 1993;

Teasdale et al., 1996; Dubé et al., 2004). The massive silicic breccia zone is located immediately underneath the thickest portion of the Au-rich massive sulfide deposit (Teasdale et al., 1996) and clasts of highly silicic altered rock are present within the ore (Fig. 14D). The higher gold grades are typically associated with the presence of bornite (Fig. 14H; Tourigny et al., 1993, Teadale et al., 1996). As at LaRonde Penna, the andalusite-rich and massive silicic zones are thought to have been produced by intense acid leaching (Teasdale et al., 1996; Dubé et al., 2004). The similar styles of mineralization and alteration mineral assemblages at LaRonde Penna and Bousquet 2-Dumagami are thought to reflect a single hydrothermal system (Fig. 18) in which variable contributions of hydrothermal seawater and magmatic volatiles contributed to the different styles of alteration and mineralization. In areas of most intense acid alteration, where the magmatic contribution could have been more important similar to high-sulfidation deposits, the transport of Cu and Au appears to have been enhanced (e.g., Bousquet 2). The upper and intermediate parts of the LaRonde Penna mine represent a hybrid, distant from the potential magmatic fluid source, whereas the Bousquet 2-Dumagami and the deeper portion of LaRonde Penna (aluminous zone) were closer to the source and share the characteristics of high-sulfidation–type Au-rich VMS (e.g., Sillitoe et al., 1996). Thus, the diverse styles of Au-rich VMS recognized by Sillitoe et al. (1996) and Hannington et al. (1999) can coexist laterally within the same deposit as well as in different deposits within a district.
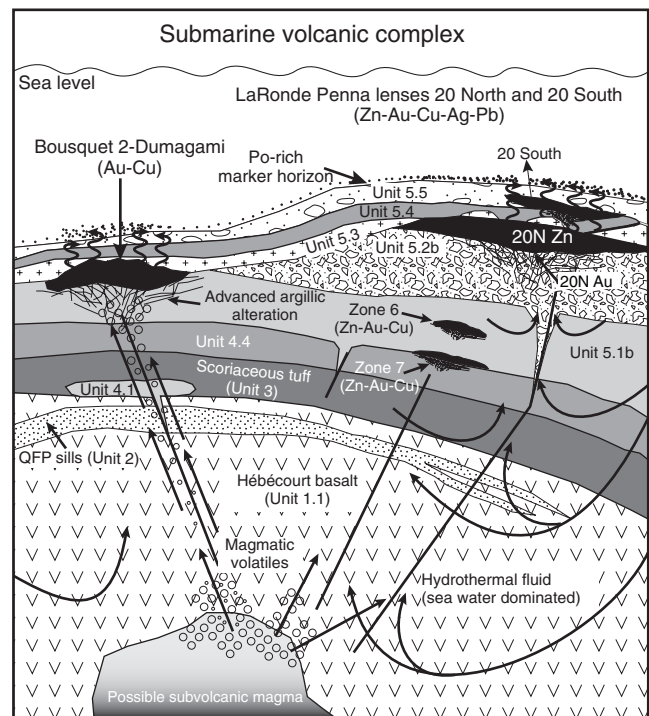

FIG. 18. Schematic east-west section, showing the possible predeformation architecture of the mineralized hydrothermal system in the LaRonde-Bousquet 2 Au-rich VMS complex in relationship to the simplified stratigraphy (modified from Dubé et al., 2004).

Comparison with high-sulfidation subaerial epithermal systems

The absence of high-sulfidation state minerals like enargite and luzonite as well as hypogene alunite and vuggy silica clearly distinguishes the LaRonde-Bousquet 2 Au-rich VMS hydrothermal system from subaerial high-sulfidation epithermal systems (e.g., Arribas, 1995; Hedenquist et al., 1994, 1996, 2000). The absence of vuggy silica could be a function of the submarine environment in which the deposit formed. However, the Cu-Au association, the advanced argillic alteration, and the local strongly silicified zone at Bousquet 2 (Fig. 14G) are very similar in mineralogy and geochemistry to some metamorphosed high-sulfidation epithermal deposits (e.g., Hope Brook, Newfoundland: Dubé et al., 1998). At Bousquet 2, the size of the silicic alteration zone is much smaller than in subaerial epithermal deposits but this could be related to the buffering of the acidic fluid by seawater. The geologic setting characterized by calc-alkaline intermediate to felsic volcanic rocks is also very typical of subaerial high-sulfidation epithermal deposits (Hedenquist et al., 1996).

Exploration guidelines

As originally recognized at the Bousquet 1 deposit, the manganiferous garnet zone provides a useful mineralogical and lithogeochemical guide to ore in the district (Valliant and Barnett, 1982; Marquis et al., 1990a, c; Tourigny et al., 1993). The quartz-biotite-manganese-rich garnet alteration zone in transitional to calc-alkaline dacite-rhyodacite volcaniclastic-volcanic rocks represents the proximal footprint of the hydrothermal alteration system, especially in the footwall of the 20 North zone at the upper and middle levels of the mine. The andalusite-kyanite–rich aluminous alteration is a key vector or the actual host to ore at depth at LaRonde Penna and at the Bousquet 2-Dumagami and Bousquet 1 deposits. These variations in hydrothermal assemblages indicate significant variations in the nature of the hydrothermal fluids. At LaRonde Penna, the auriferous mineralized zones are not restricted to the massive sulfide lenses, as recognized elsewhere for Au-rich VMS deposits (Huston, 2000).

The emplacement of several felsic domes in the area (units 5.1b, 5.2b, 5.3, and 5.5) most probably contributed to the longevity of the thermal gradient in the immediate environment and allowed development of stacked sulfide lenses throughout the Bousquet Formation. Thus, proximity of transitional to calc-alkaline volcanic centers is a key element in terms of exploration in the district and distinguishes the LaRonde Penna and Bousquet 2-Dumagami deposits from typical Archean VMS environments (Barrie et al., 1993, Hart et al., 2004, Mercier-Langevin et al., 2007a). Almost all sulfide lenses or hydrothermal alteration zones are located at or near stratigraphic breaks within the Bousquet Formation. These breaks represent major exploration targets, especially when located in the upper part of the Bousquet Formation. Volcanic hiatuses with a presence of the basaltic andesite (unit 5.4) or the feldspar- and quartz-phyric rhyolite (unit 5.3) in the hanging wall are particularly prospective. Because of their ductility, the aluminous alteration zones have accommodated most of the postore strain. These alteration zones are commonly transposed subparallel to high-strain zones and transformed into schists. Consequently, the alteration spatially coincides with deformation zones, although there are no genetic relationships. Quartz-Mn–rich garnet-biotite assemblage and/or aluminous schists with anomalous gold and/or zinc values in intermediate to felsic transitional to calc-alkaline volcanic or volcaniclastic rocks located underneath a sedimentary cover are considered to be among the most prospective targets for Au-rich VMS in metamorphosed terranes.

Acknowledgments

REFERENCES

Allen, R.A., Weihed, P., and Svenson, S.A., 1996, Setting of Zn-Cu-Au-Ag massive sulfide deposits in the evolution and facies architecture of the 1.9 Ga marine volcanic arc, Skellefte district, Sweden: ECONOMIC GEOLOGY, v. 91, p. 1022–1053.

Arnold, G.O., and Sillitoe, R.H., 1989, Mount Morgan gold-copper deposit, Queensland, Australia: Evidence for an intrusion-related replacement origin: ECONOMIC GEOLOGY, v. 84, p. 1805–1816.

Arribas, A., Jr., 1995, Characteristics of high-sulfidation epithermal deposits, and their relation to magmatic fluid: Mineralogical Association of Canada Short Course Handbook 23, p. 419–454.

Barrett, T.J., and MacLean, W., 1994, Chemostratigraphy and hydrothermal alteration in exploration for VHMS deposits in greenstones and younger volcanic rocks: Geological Association of Canada, Mineral Deposits Division, Short Course Notes, v. 11, p. 433–467.

Barrie, C.T., and Hannington, M.D., 1999, Classification of volcanic-associated massive sulfide deposits based on host-rock composition, Reviews in Economic Geology, v. 8, p. 1–11.

Barrie, C.T., Ludden, J.N., and Green, T.H., 1993, Geochemistry of volcanic rocks associated with Cu-Zn and Ni-Cu deposits in the Abitibi subprovince: ECONOMIC GEOLOGY, v. 88, p. 1341–1358.

Bergman Weihed, J., Bergstrom, U., Billstrom, K., and Weihed, P., 1996, Geology, tectonic setting, and origin of the Paleoproterozoic Boliden Au-Cu-As deposit, Skellefte district, northern Sweden: ECONOMIC GEOLOGY, v. 91, p. 1073–1097.

Callaghan, T., 2001, Geology and host-rock alteration of the Henty and Mount Julia gold deposits, Western Australia: ECONOMIC GEOLOGY, v. 96, p. 1073–1088.

Davis, D.W., 2002, U-Pb geochronology of Archean metasedimentary rocks in the Pontiac and Abitibi subprovinces, Quebec: Constraints on timing, provenance and regional tectonics: Precambrian Research, v. 115, p. 97–117.

Dimroth, E., Imreh, L., Goulet, N., and Rocheleau, M., 1983, Evolution of the south-central part of the Archean Abitibi belt, Quebec. Part II: Tectonic evolution and geomechanical model: Canadian Journal of Earth Sciences, v. 19, p. 1729–1758.

Doyle, M.G., and Allen, R.L., 2003, Subsea-floor replacement in volcanic-hosted massive sulfide deposits: Ore Geology Reviews, v. 23, p. 183–222.

Dubé, B., Dunning, G., and Lauzière, K., 1998, Geology of the Hope Brook mine, Newfoundland, Canada: A preserved Late Proterozoic high-sulfidation epithermal gold deposit and its implications for exploration: ECONOMIC GEOLOGY, v. 93, p. 405–436.

Dubé, B., Mercier-Langevin, P., Lafrance, B., Hannington, M., Moorhead, J., Davis, D., and Pilote, P., 2003, The Doyon-Bousquet-LaRonde Archean Au-rich VMS gold camp: the example of the world-class LaRonde deposit, Abitibi, and its implications for exploration [abs.]: Canadian Institute of Mining and Metallurgy, 2003 Field Conference, Ore Deposits at Depth: Challenges and Opportunities, September 23–26, Technical Sessions Abstract Volume, p 3–10.

Dubé, B., Mercier-Langevin, P., Hannington, M.D., Davis, D.W., and Lafrance, B., 2004, Le gisement de sulfures massifs volcanogènes aurifères LaRonde, Abitibi, Québec : altération, minéralisation, genèse et implications pour l'exploration. Ministère des Ressources Naturelles, Faune et Parcs, Québec, Report MB 2004–03, 112 p.

Franklin, J.M., 1996, Volcanic-associated massive sulphide base metals: Geological Survey of Canada, Geology of Canada, no. 8, The Geology of North America v. P-1, p. 158–183.

Franklin, J.M., Sangster, D.F., and Lydon, J.W., 1981, Volcanic-associated massive sulfide deposits: ECONOMIC GEOLOGY 75TH ANNIVERSARY VOLUME, p. 485–627.

Galley, A.G., Bailes, A.H., and Kitzler, G. 1993, Geological setting and hydrothermal evolution of the Chisel Lake and North Chisel Zn-Pb-Cu-Ag-Au massive sulfide deposits, Snow Lake, Manitoba: Exploration and Mining Geology, v. 2, p. 271–295.

Galley, A.G., Pilote, P., and Davis, D., 2003, Gold-related subvolcanic Mooshla intrusive complex, Bousquet mining district, P.Q. [abs.]: Canadian Institute of Mining and Metallurgy, 2003 Field Conference, Ore Deposits at Depth: Challenges and Opportunities, September 23–26, Technical Sessions Abstract Volume, p. 16.

Gemmell, J.B., and Fulton, R., 2001, Geology, genesis, and exploration implications of the footwall and hanging-wall alteration associated with the Hellyer volcanic-hosted massive sulfide deposit, Tasmania, Australia: ECONOMIC GEOLOGY, v. 96, p. 1003–1035.

Gibson, H.L., and Watkinson, D.H., 1990, Volcanogenic massive sulphide deposits of the Noranda cauldron and shield volcano, Quebec: Canadian Institute of Mining and Metallurgy Special Volume 43, p. 119–132.

Gosselin, G., 1998, Veines de quartz aurifères précoces à la zone Ouest de la Mine Doyon, Canton de Bousquet, Preissac, Abitibi: Unpublished M.Sc. thesis, Université du Québec à Chicoutimi, 128 p.

Gosselin, P., and Dubé, B., 2005a, Gold deposits of the world: Distribution, geological parametres and gold content: Geological Survey of Canada Open-File Report 4895, 214 p.

——2005b, Gold deposits of Canada: Distribution, geological parametres and gold content: Geological Survey of Canada Open-File Report 4896, 64 p.

Grant, J.A., 1986, The Isocon diagram-A simple solution to Gresen's equation for metasomatic alteration: ECONOMIC GEOLOGY, v. 81, p. 1976–1982.

Gunning, H.G., 1941, Bousquet-Joannes area, Quebec: Geological Survey of Canada Memoir 231, 110 p.

Hallberg, A., 2001, Rock classification, magmatic affinity, and hydrothermal alteration at Boliden, Skellefte disrict, Sweden—a desk-top approach to whole rock geochemistry: Geological Survey of Sweden, Economic Geology Research, v. 1, Research Paper C 833, p. 93–131.

Hannington, M.D., Poulsen, K.H., Thompson, J.F.H., and Sillitoe, R., 1999, Volcanogenic gold in the massive sulfide environment: Reviews in Economic Geology, v. 8, p. 325–356.

Hart, T., Gibson, H.L., and Lesher, C.M., 2004, Trace element geochemistry and petrogenesis of felsic volcanic rocks associated with volcanogenic Cu-Zn-Pb massive sulfide deposits: ECONOMIC GEOLOGY, v. 99, p. 1003–1013.

Hedenquist, J.W., and Lowenstern, J.B., 1994, The role of magmas in the formation of hydrothermal ore deposits: Nature, v. 370, p. 519–527.

Hedenquist, J.W., Matsuhia, Y., Izawa, E., White, N.C., Giggenbach, W.F., and Aoki, M., 1994, Geology, geochemistry, and origin of high-sulfidation Cu-Au mineralization in the Nansatsu district, Japan: ECONOMIC GEOLOGY, v. 89, p. 1–30.

Hedenquist, J.W., Izawa, E., Arribas, A., Jr., and White, N.C., 1996, Epithermal gold deposits: Styles, characteristics, and exploration: Resource Geology Special Publication 1, 17 p. (Poster and booklet, with translations to Spanish, French, Japanese, and Chinese).

Hedenquist, J.W., Arribas, A., Jr., and Gonzalez-Urien, E., 2000, Exploration for epithermal gold deposits: Reviews in Economic Geology, v. 13, p. 245–277.

Hubert, C., Trudel, P., and Gélinas, L., 1984, Archean wrench fault tectonics and structural evolution of the Blake River Group, Abitibi belt, Quebec: Canadian Journal of Earth Sciences, v. 21, p. 1024–1032.

Huston, D.L., 1993, The effect of alteration and metamorphism on wall rocks to the Balcooma and Dry River South volcanic-hosted massive sulfide deposits, Queensland, Australia: Journal of Geochemical Exploration, v. 48, p. 277–307.

——2000, Gold in volcanic-hosted massive sulfide deposits: Distribution, genesis and exploration: Reviews in Economic Geology, v. 13, p. 401–426.

Huston, D.L., and Kamprad, J., 2000, The Western Tharsis deposit: A "high-sulfidation" Cu-Au deposit in the Mt Lyell field, western Tasmania, of possible Ordovician age: Australian Geological Survey Organisation Research Newsletter 32, p. 2–6.

Huston, D.L., and Large, R.R., 1988, Distribution, mineralogy, and geochemistry of gold and silver in the North End orebody, Rosebery, Tasmania: ECONOMIC GEOLOGY, v. 83, p. 1181–1192.

——1989, A chemical model for the concentration of gold in volcanogenic massive sulphide deposits: Ore Geology Reviews, v. 4, p. 171–200.

Huston, D.L., and Paterson, D.J., 1995, Zincian staurolite in the Dry River South volcanic-hosted massive sulfide deposit, northern Queensland, Australia: An assessment of its usefulness in exploration: Applied Geochemistry, v. 10, p. 329–336.

Huston, D.L., Bottrill, R.S., Creelman, R.A., Khin Zaw, Ramsden, T.R., Rand, S.W., Gemmell, J.B., Jablonski, W., Sie, S.H., and Large, R.R., 1992, Geologic and geochemical controls on the mineralogy and grain size of gold-bearing phases, eastern Australian volcanic-hosted massive sulfide deposits: ECONOMIC GEOLOGY, v. 87, p. 542–563.

Ishikawa, Y., Sawaguchi, T., Iwaya, S., and Horiuchi, M., 1976, Delineation of prospecting targets for Kuroko deposits based on modes of volcanism of underlying dacite and alteration haloes: Mining Geology; v. 26, p. 105–117.

Lafrance, B., Moorhead, J., and Davis, D., 2003, Cadre géologique du camp minier de Doyon-Bousquet-LaRonde: Ministère des Ressources Naturelles, Québec, ET 2002–07, 45 p.

Lafrance, B., Davis, D.W., Goutier, J., Moorhead, J., Pilote, P., Mercier-Langevin, P., Dubé, B., Galley, A.G., and Mueller, W.U., 2005, Nouvelles datations isotopiques dans la portion québécoise du Groupe de Blake River et des unités adjacentes: Ressources Naturelles et Faune Québec, RP 2005–01, 15 p.

Large, R.R., McPhie, J., Gemmell, J.B., Herrmann, W., and Davidson, G.J., 2001, The spectrum of ore deposit types, volcanic environments, alteration halos, and related exploration vectors in submarine volcanic successions: Some examples from Australia: ECONOMIC GEOLOGY, v. 96, p. 913–938.

Marquis, P., Hubert, C., Brown, A.C., and Rigg, D.M., 1990a, Overprinting of early, redistributed Fe and Pb-Zn mineralization by late-stage Au-Ag-Cu deposition at the Dumagami mine, Bousquet district, Abitibi, Quebec: Canadian Journal of Earth Sciences, v. 27, p. 1651–1671.

——1990b, An evaluation of genetic models for gold deposits of the Bousquet district, Quebec, based on their mineralogic, geochemical, and structural characteristics: Canadian Institute of Mining and Metallurgy Special Volume 43, p. 383–399.

Marquis, P., Brown, A.C., Hubert, C., and Rigg, D.M., 1990c, Progressive alteration associated with auriferous massive sulfide bodies at the Dumagami mine, Abitibi greenstone belt, Quebec: ECONOMIC GEOLOGY, v. 85, p. 746–764.

Mercier-Langevin, P., 2005, Géologie du gisement de sulfures massifs volcanogènes aurifères LaRonde, Abitibi, Québec: Unpublished Ph.D. thesis, Institut national de la recherche scientifique, Eau, Terre et Environnement, 694 p.

Mercier-Langevin, P., Dubé, B., Hannington, M.D., Davis, D., and Lafrance, B., 2004, Contexte géologique et structural des sulfures massifs volcanogènes aurifères du gisement LaRonde, Abitibi : Ministères des Ressources Naturelles de la Faune et des Parcs, ET 2003–03, 60 p.

Mercier-Langevin, P., Dubé, B., Hannington, M.D., Davis, D.W., Lafrance, B., and Gosselin, G., 2007a, The LaRonde Penna Au-rich volcanogenic massive sulfide deposit, Abitibi greenstone belt, Quebec: Part I. Geology and geochronology: ECONOMIC GEOLOGY, v. 102, p. 585–609.

Mercier-Langevin, P., Dubé, B., Hannington, M.D., Richer-Laflèche, M., and Gosselin, G., 2007a, The LaRonde Penna Au-rich volcanogenic massive sulfide deposit, Abitibi greenstone belt, Quebec: Part II. Lithogeochemistry and paleotectonic setting: ECONOMIC GEOLOGY, v. 102, p. 611–631.

Mercier-Langevin, P., Dubé, B., Lafrance, B., Hannington, M.D., Galley, A., and Moorhead, J., 2007b, A group of papers devoted to the LaRonde Penna Au-rich volcanogenic massive sulfide deposit, eastern Blake River Group, Abitibi greenstone belt, Quebec—Preface: ECONOMIC GEOLOGY, v. 102, p. 577–583.

Morton, R.L., and Franklin, J.M., 1987, Two-fold classification of Archean volcanic-associated massive sulfide deposits: ECONOMIC GEOLOGY, v. 82, p. 1057–1063.

Nilsson, C.A., 1968, Wall rock alteration at the Boliden deposit, Sweden: ECONOMIC GEOLOGY, v. 63, p. 472–494.

Ödman, O.H., 1941, Geology and ores of the Boliden deposit, Sweden: Sveriges Geologiska Undersökning, Series C, v. 438, 190 p.

Ohmoto, H., 1996, Formation of volcanogenic massive sulfide deposits: the Kuroko perspective: Ore Geology Reviews, v. 10, p. 135–177.

Poulsen, K.H., and Hannington, M.H., 1995, Volcanic-associated massive sulfide gold: Geological Survey of Canada, Geology of Canada, no. 8, The Geology of North America v. P-1, p. 183–196.

Poulsen, K.H., Robert, F., and Dubé, B., 2000, Geological Classification of Canadian gold deposits: Geological Survey of Canada Bulletin 540, 106 p.

Powell, W.G., Carmichael, D.M., and Hodgson, C.J., 1995, Conditions and timing of metamorphism in the southern Abitibi greenstone belt, Quebec: Canadian Journal of Earth Sciences. v. 32, p. 787–805.

Rickard, D., ed., 1986, The Skellefte fields: Sveriges Geologiska Undersökning, Series Ca, v. 62, 54 p.

Ririe, G.T., 1990, A comparison of alteration associated with Archean gold deposits in Western Australia and Paleozoic gold deposits in the southeast United States: Canadian Journal of Earth Sciences, v. 27, p. 1560–1576.

Sillitoe, R.H., Hannington, M.D., and Thompson, J.F., 1996, High-sulfidation deposits in the volcanogenic massive sulfide environment: ECONOMIC GEOLOGY, v. 91, p. 204–212.

Stone, W.E., 1988, Nature and significance of metamorphism in gold concentration, Bousquet township, Abitibi greenstone belt, northwest Quebec: Unpublished Ph.D thesis, London, University of Western Ontario, 441 p.

——1990, Archean volcanism and sedimentation in the Bousquet gold district, Abitibi greenstone belt, Quebec: Implications for stratigraphy and gold concentration: Geological Society of America Bulletin, v. 102, p. 147–158.

Stone, W.E., Valliant, R.I., and Bateman, P.W., 1988, Wall rock alteration, regional metamorphism and gold concentration in the Bousquet gold district, Abitibi greenstone belt, Quebec, Canada [ext. abs.]: Bicentennial Gold'88, Extended Abstracts Oral Programme, Geological Society of Australia, Abstracts 22, p. 51–55.

Teasdale, N., Brown, A.C., and Tourigny, G., 1996, Gîtologie de la mine Bousquet 2: Ministère des Ressources Naturelles, Québec, MB 96–37, 43 p.

Tourigny, G., Brown, A.C., Hubert, C., and Crepeau, R., 1988, Structural geology of the Blake River Group at the Bousquet mine, Abitibi, Quebec: Canadian Journal of Earth Sciences, v. 25, p. 581–592.

——1989, Synvolcanic and syntectonic gold mineralization at the Bousquet mine, Abitibi greenstone belt: ECONOMIC GEOLOGY, v. 84, p. 1875–1890.

Tourigny, G., Doucet, D., and Bourget, A., 1993, Geology of the Bousquet 2 mine: An example of a deformed, gold-bearing, polymetallic sulfide deposit: ECONOMIC GEOLOGY, v. 88, p. 1578–1597.

Valliant, R.I., and Barnett, R.L., 1982, Manganiferous garnet underlying the Bousquet gold orebody, Quebec: Metamorphosed manganese sediment as a guide to gold ore: Canadian Journal of Earth Sciences, v. 19, p. 993–1010.

Valliant, R.I., and Hutchinson, R.W., 1982, Stratigraphic distribution and genesis of gold deposits, Bousquet region, Northwestern Quebec: Canadian Institute of Mining and Metallurgy Special Volume 24, p. 27–40.

Valliant, R.I., Barnett, R.L., and Hodder, R.W., 1983, Aluminum silicate-bearing rock and its relation to gold mineralization, Bousquet mine, Bousquet township, Quebec: Canadian Institute of Mining and Metallurgy Bulletin, v. 76, no. 850, p. 81–90.

Williams, N.C., and Davidson, G.J., 2004, Possible submarine advanced argillic alteration at the Basin Lake prospect, western Tasmania, Australia: ECONOMIC GEOLOGY, v. 99, pp. 987–1002.

Yeats, C.J., and Groves, D.I., 1998, The Archean Mount Gibson gold deposits, Yilgarn craton, Western Australia: Products of combined synvolcanic and syntectonic alteration and mineralisation: Ore Geology Reviews, v. 13, p. 103–129.